Resource

Stable expansion of high-grade serous ovarian cancer organoids requires a low-Wnt environment

Karen Hoffmann[1,†], Hilmar Berger[1], Hagen Kulbe[2], Sukanija Thillainadarasan[1], Hans-Joachim Mollenkopf[1], Tomasz Zemojtel[3], Eliane Taube[4], Silvia Darb-Esfahani[4], Mandy Mangler[5], Jalid Sehouli[2], Radoslav Chekerov[2], Elena I Braicu[2], Thomas F Meyer[1,*] & Mirjana Kessler[1,†,**]

Abstract

High-grade serous ovarian cancer (HGSOC) likely originates from the fallopian tube (FT) epithelium. Here, we established 15 organoid lines from HGSOC primary tumor deposits that closely match the mutational profile and phenotype of the parental tumor. We found that Wnt pathway activation leads to growth arrest of these cancer organoids. Moreover, active BMP signaling is almost always required for the generation of HGSOC organoids, while healthy fallopian tube organoids depend on BMP suppression by Noggin. Fallopian tube organoids modified by stable shRNA knockdown of p53, PTEN, and retinoblastoma protein (RB) also require a low-Wnt environment for long-term growth, while fallopian tube organoid medium triggers growth arrest. Thus, early changes in the stem cell niche environment are needed to support outgrowth of these genetically altered cells. Indeed, comparative analysis of gene expression pattern and phenotypes of normal vs. loss-of-function organoids confirmed that depletion of tumor suppressors triggers changes in the regulation of stemness and differentiation.

Introduction

High-grade serous ovarian cancer (HGSOC), an occult malignancy which represents 70% of all ovarian cancer cases and has the highest mortality rates (5-year survival rate 30–40%) (Reid *et al*, 2017), represents a major clinical challenge. Aside from the difficulties in developing new lines of targeted treatments, late detection and lack of understanding of the molecular mechanisms that drive development of the disease remain major hurdles. Studies in BRCA1/2 germ-line mutation carriers undergoing prophylactic cancer risk-reducing surgery (Leeper *et al*, 2002; Callahan *et al*, 2007) identified distinct early malignant changes in the distal part of the FT, leading to widespread acceptance of the theory that the FT is the primary tissue of origin of HGSOC (Vaughan *et al*, 2011; Bowtell *et al*, 2015). These lesions, termed small tubal intraepithelial carcinoma (STIC), are also routinely detected in the FT epithelium of ~ 50% of patients at an advanced stage of the disease and were shown to have the same genomic profile as the mature cancer—indicative of a clonal relationship (Kuhn *et al*, 2012). Nevertheless, all tumor samples genomically and transcriptionally cluster together and closely resemble tubal epithelium, irrespective of whether STICs were detected in the FT (Ducie *et al*, 2017). Therefore, it remains unclear how cellular transformation occurs, and most importantly, which factors are essential for the development of invasive and metastatic properties, which are necessary for the spread of malignant cells from the FT to the ovary and beyond. Of particular interest in this context is the role of mutant p53, which is almost universally detected in metastatic HGSOC cancers (Cancer Genome Atlas Research Network, 2011), but can occasionally be found in the form of p53 signatures in healthy patients with unclear clinical significance (Lee *et al*, 2007). Thus, it cannot be excluded that the occurrence of mutated p53 is coupled to additional, independent transformation stimuli that provide a selective advantage during the process of transformation.

Several studies have investigated drug responses of different patient-derived 3D models of HGSOC in short-term culture, but conditions suitable for stable long-term cultivation and creation of biobanks have remained elusive (Hill *et al*, 2018; Maru *et al*, 2019; Phan *et al*, 2019). The recently reported generation of organoid cultures from ovarian cancer (Kopper *et al*, 2019) demonstrated that it is possible, in principle, to maintain the major properties of ovarian cancer tissue *in vitro*. Notably, while providing a comprehensive

1 Department of Molecular Biology, Max Planck Institute for Infection Biology, Berlin, Germany
2 Department of Gynecology, Charité University Medicine, Campus Virchow-Klinikum, Berlin, Germany
3 BIH Genomics Core Unit, Charité University Medicine, Campus Virchow-Klinikum, Berlin, Germany
4 Department of Pathology, Charité University Medicine, Campus Charité, Berlin, Germany
5 Department of Gynecology, Vivantes Auguste-Viktoria-Klinikum, Berlin, Germany
*Corresponding author. Tel: +49 3028 460400; E-mail: tfm@mpiib-berlin.mpg.de
**Corresponding author. Tel: +49 3045 0653504; E-mail: mirjana.kessler@charite.de
†Present address: Department of Internal Medicine/Infectious Diseases and Pulmonary Medicine, Charité University Medicine, Berlin, Germany

overview of the different histological subtypes and stages of the disease, only two cases (five lines in total) from the reported cohort involved samples from primary surgery, while the remainder were pre-exposed to neoadjuvant chemotherapy. Interestingly, four out of five primary HGSOC organoid lines exhibited slow growth, suggesting suboptimal culture conditions. To date, it remains unclear how the stem cell niche is altered in the native HGSOC tumor tissue compared to healthy epithelium. Here, we define growth conditions needed to achieve stable, long-term expansion of HGSOC organoids from primary tumor deposits. We show that the niche composition for stemness maintenance of cancer organoids requires low-Wnt signaling and benefits from active BMP signaling, which is in contrast to the paracrine environment that regulates epithelial homeostasis in healthy FT organoids (Kessler *et al*, 2015).

In total, we have created 15 stable organoid lines from 13 primary deposits of advanced HGSOC patients, which match the mutational and phenotypic profile of the parental tumor. In parallel, we have generated FT organoid cultures from seven different patients with simultaneous depletion of p53, PTEN, and RB (triple shRNA knockdowns), leading to the disruption of major signaling pathways that have been implicated in HGSOC development. Importantly, long-term growth of triple KD organoids could only be sustained in medium adapted for HGSOC organoids. Comparative gene expression analysis of cancer organoids and p53/PTEN/RB triple KDs under different growth conditions revealed common key regulatory changes in markers of stemness and differentiation. This implies that signaling cues from the stem cell environment need to change early during tumorigenesis to facilitate the growth of mutated cells and are preserved in the advanced disease setting. Thus, this study discovers important core principles in the development of HGSOC, which have important implications for understanding early carcinogenesis and disease progression.

Results

Establishment of HGSOC organoid culture

In order to define conditions for long-term *in vitro* propagation of primary cancer organoids from solid HGSOC deposits, we utilized a combinatorial screening approach, using samples obtained during primary debulking surgery. To avoid potential contribution from healthy fallopian tube or ovarian surface epithelium, only tumor samples from peritoneum and omentum deposits were used. The tissue was not pre-exposed to pharmacological agents, as all but one HGSOC patient underwent radical surgery prior to chemotherapy, in line with local clinical guidelines. Small pieces (1–3 cm) of suspected tumor mass identified by the surgeon were transported to the lab and subjected to cell isolation on the same day. 3D culture was initiated by seeding the cell suspension in Matrigel and supplementation with growth factors (for details see Methods and Protocols). Overall, 15 organoid lines were successfully established from 13 out of 45 patients (~ 30% efficiency), which were classified based on TNM and FIGO staging (Table EV1). The majority had cancer deposits of > 2 cm that had invaded organs outside the pelvis (T3c) and spread to retroperitoneal lymph nodes (N1), but had not metastasized to more distant sites such as the liver or spleen (M0) (Fig 1A). In order to generate a reference data set for

each organoid line, the parental tumor sample was divided into three parts for (i) confirmation of the diagnosis by an experienced pathologists using histological analysis of standard HGSOC biomarkers (Fig EV1A), (ii) isolation of DNA and RNA, and (iii) isolation of cells for organoid culture (Fig 1B).

By testing media containing different combinations of growth factors (Fig 1C), we identified conditions that support outgrowth and long-term expansion (> 1 year) of cancer-derived organoids. Normal FT organoid medium (FTM) (Table EV2) is supplemented with ROCK and TGF-β receptor inhibitors, as well as Noggin, EGF, FGF, RSPO1, and Wnt3a (Kessler *et al*, 2015; Kopper *et al*, 2019). By contrast, HGSOC organoids did not grow in this medium but required several alterations. The only paracrine growth factor that proved indispensable was EGF (E). Most notably, unlike healthy organoids from several different organs (intestinal, FT, gastric, liver, etc.), which require exogenous Wnt activation, not a single organoid line could be maintained in medium containing the Wnt signaling agonist Wnt3a (W) (Fig 1C and Table EV3). Two lines did, however, expand in the presence of the Wnt agonist R-spondin 1 (RSPO1, short R), suggesting that some cultures benefit from the addition of RSPO1 (Fig 1C). In addition, sustained inhibition of BMP signaling by Noggin (N) seems to be detrimental, as removal of Noggin was a prerequisite for successful cultivation in 13/15 HGSOC samples, indicating fundamentally different roles of BMP and Wnt signaling in the regulation of stemness in HGSOC compared to normal tissue. Indeed, activation of Wnt pathway by GSK3-β inhibitor CHIR99201 (CHIR), instead of addition of Wnt3a agonist, also showed clear negative effect on organoid formation and growth supporting conclusion that regulation of stemness potential in HGSOC tissue has altered requirement for Wnt signal (Fig EV1B). In summary, 11/15 cultures could be initiated and expanded in medium containing only EGF, ROCK, and TGF-β inhibitors, but without Noggin—thus allowing endogenous BMP signaling (Table EV3). Five of these 11 samples benefited from the addition of BMP2 for organoid formation, further amplifying BMP signaling (B). As this patient-dependent effect of BMP2 addition was always neutral or positive, BMP2 was subsequently included in the standard medium composition. Therefore, the combination of EGF and BMP2, together with other standard components of organoid medium, i.e., ROCK inhibitor, TGF-β inhibitor, B27, N2, and nicotinamide (consistent with Kopper *et al*, 2019), was termed ovarian cancer minimal medium (OCM) (Table EV3).

Successfully established long-term HGSOC organoid cultures were passaged at a ratio of 1:2 to 1:3 every 10–20 days for at least 5 months prior to cryopreservation. Six lines were kept in culture for > 1 year (Table EV3). Thawed cancer organoids could routinely be expanded to a multi-well screening format and are thus suited for generating live biobanks of HGSOC organoids to explore individual therapeutic options *in vitro*. Multiple cycles of thawing and freezing were tested on seven different lines without noticeable changes in morphology or expansion potential.

Immunofluorescence labeling confirmed that the organoids exhibit all hallmarks of an HGSOC phenotype, including disorganized tissue architecture and loss of polarity (as marked by the absence of a central cavity), an epithelial secretory identity of all cells (strong EpCAM and PAX8 expression), and pleomorphic nuclei (Fig 1D). HE staining further confirmed their morphological similarity to the matching tissue samples (Fig 1E). Next, we tested the
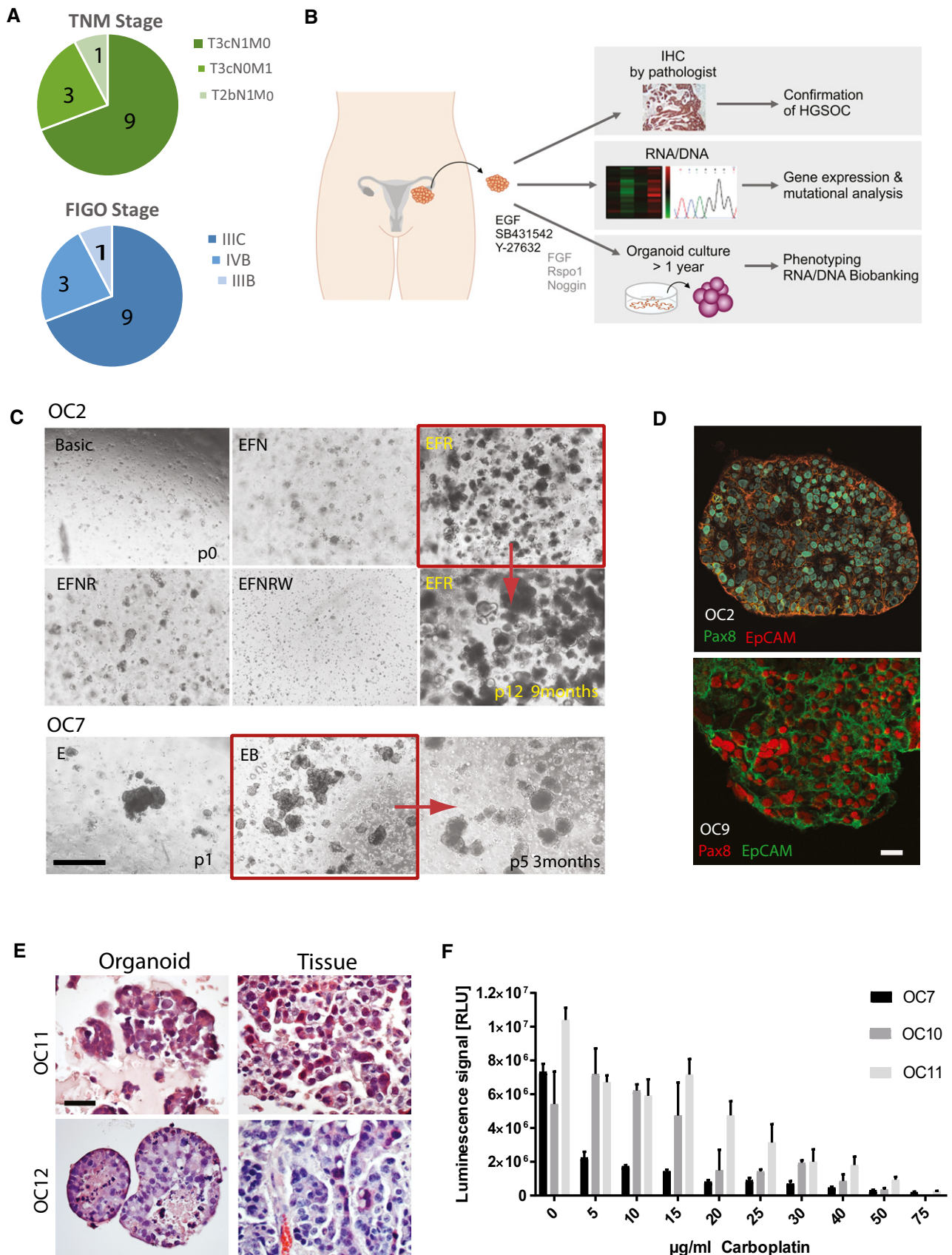
Figure 1.

Figure 1. Establishment of patient-derived organoids from solid HGSOC deposits.

A   Summary of cancer patient data with TNM and FIGO classifications showing advanced stage of disease at the time of surgery.
B   Graphic representation of the standard experimental procedure for tumor patient material. Samples were obtained at the time of primary debulking surgery from the high purity tumor deposits in peritoneum/omentum.
C   *In vitro* niche dependency of HGSOC tumor cells. Phase-contrast pictures illustrate that isolated ovarian cancer cells rely on EGF supplementation for growth, while they do not grow at all in Wnt3a-supplemented medium. Also, inhibition of BMP signaling through Noggin has strong negative effect on the initial growth. Scale bar: 500 μm. E—EGF, F—FGF10, N—Noggin, R—R-spondin1, B—Basic medium, P—Passage.
D   Cancer organoids express HGSOC markers Pax8 and EpCAM and have lost the cystic phenotype suggesting complete breakdown of epithelial polarity as seen on confocal images from two representative organoid lines. Scale bar: 20 μm.
E   HE staining of organoids and respective tissue confirms high similarity in cellular structure and tissue organization. Scale bar: 100 μm.
F   HGSOC organoids show differential response to carboplatin treatment, confirming patient-specific sensitivity of the cultures. Cell viability assay was performed after 5 days of treatment with different concentrations of carboplatin on mature organoids from three different donors. Data represent mean ± SD of technical triplicates.

in vitro drug response to carboplatin, the major first-line chemotherapeutic agent for HGSOC. As expected, organoids underwent cell death in a concentration-dependent manner, with prominent differences between organoids from different donors suggesting individual variation in drug response among patients (Figs 1F and EV1C).

HGSOC organoids match tumor tissue in mutational profile and expression of biomarkers

To test whether patient-derived organoid cultures correspond to the individual mutational profile of the parental tumor, we performed targeted sequencing for 121 candidate genes that were selected on the basis of previously published studies of ovarian cancer genomic profiles (Appendix Table S1; Cancer Genome Atlas Research Network, 2011, Norquist *et al*, 2018). Mutational analysis of 10 paired tumor fragments and organoids from nine different patients revealed that despite the long-term expansion *in vitro* (DNA samples were collected after 4–10 months in culture, see Table EV3), they retained a high level of similarity, even including allelic frequency, when compared to the tissue that was immediately frozen on the day of surgery (Fig 2A and Table EV4). *TP53* mutations were detected in the vast majority of samples (9/10), in agreement with the almost universal occurrence of mutated p53 in HGSOC patients (Cancer Genome Atlas Research Network, 2011). All of the *TP53* mutations in the organoid cultures were homozygous (> 0.9 allele frequency), yet diverse with respect to mutation type (missense, nonsense, frame-shift, or splice variant mutations). In addition to somatic mutations with proven tumorigenic potential, a number of known variant alleles were identified, including *ROCK2* (c.1292C>A), *KIT* (c.1621A>C), *MLH1* (c.655A>G), and *MSH6* (c.472C>T) which could potentially influence the malignant phenotype (Kalender *et al*, 2010; Nakamura *et al*, 2014; Brahmi *et al*, 2015). Apart from *TP53*, *MLH1*, and *MSH6*, we also found point mutations in other genes with functions in DNA repair and chromosome stability, including *ATM* (c.4534G>A), *ATR* (c.1517A>G), *BRIP1* (c.254T>A), and *FANCA* (c.1238G>T). Interestingly, while no classic germline or somatic BRCA1/2 mutations were detected apart from three polymorphisms that are weakly associated with ovarian cancer (c.4900A>G, c.3113A>G, c.2612C>T), analysis of protein lysates revealed a significant reduction compared to healthy FT organoids in three of eight cases (OC4, OC2, and OC3; Appendix Fig S1A and Table S2). This strongly suggests the existence of epigenetic or post-transcriptional mechanisms of BRCA1 inactivation in these cases. Altogether, 7/9 patients had mutations in one or more

DNA repair gene, in congruence with the fact that HGSOC is a cancer characterized by a particularly high incidence of genomic instability. Given our finding that HGSOC organoids could not be maintained in the presence of Wnt, we noted with interest that three missense mutations in Wnt pathway genes (Fzd9, LRP5, and TCF7L2) were identified in three different patients (Fig 2A), which could impair signal transduction and thus provide further evidence that changes in this pathway play an important role in ovarian carcinogenesis. Complementary to the sequencing data, WB and IF staining were performed to examine the mutational status and subcellular localization of p53 in the organoids (Appendix Table S2). While the nonsense mutation in OC11 as well as the splice variant and frame-shift mutations in OC4 and OC7, respectively, result in loss of p53 (Fig 2B and Appendix Table S2), the missense mutations in OC9 (p.R273H), OC10 (p.R175H), OC1 (p.V25F), and OC6 (p.V173M) result in a gain-of-function and nuclear accumulation phenotype with R273H and R175H being two of the most common mutations in ovarian cancer (Zhang *et al*, 2016; Fig 2C and Appendix Fig S1B).

To more thoroughly evaluate parallels between tissue and organoid cultures, a global gene expression analysis was performed from eight different tumor/organoid pairs as well as three healthy FT tissue/organoid pairs and two FT organoids derived from cancer patients (also classified as normal healthy tissue). The generation of a multi-dimensional-scaling plot (MDS) revealed that the distance between OC and FT organoids is smaller than between corresponding tissues, likely due to the greater complexity of tissue samples, which contain mesenchymal and endothelial components (Fig 2D). Still, despite the tissue heterogeneity, the respective OC organoids express very similar levels of the main cancer markers, like CDKN2A (p16), Muc16, and EpCAM, when compared to the parental sample (Fig 2E). Moreover, correlation analysis of FT and OC organoids (Appendix Fig S1C) shows that FT samples form a homogenous cluster and show less variability in gene expression between each other than OC organoids, which instead reflect the phenotypic diversity of ovarian tumors.

A thorough analysis of gene expression revealed that numerous hallmark genes known to be de-regulated in HGSOC are differentially expressed between OC and normal FT samples, not only in the tissue but also in the organoids (Fig 2F). This includes significant up-regulation of the cell cycle regulators CDKN2A and Cyclin E1 (CCNE1) and the transcription factor FOXM1, as well as downregulation of differentiation markers like PGR and OVGP1.

The strong up-regulation of Cyclin E1 was validated by Western blot analysis in five out of eight samples tested (Appendix Fig S1D

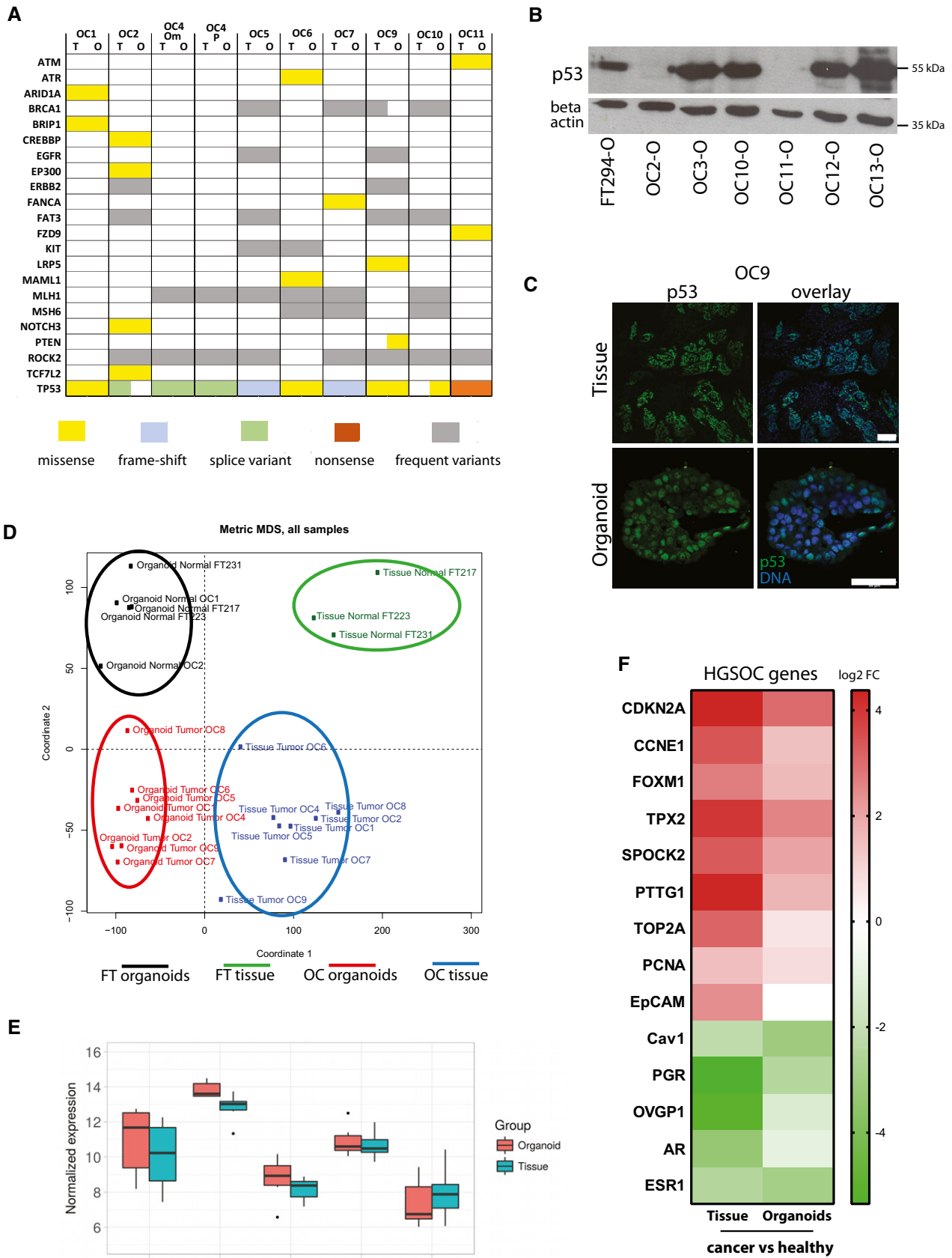**Figure 2.**

◀

Figure 2. HGSOC organoids match tumor tissue in mutational profile and gene expression biomarkers.

A Overview of mutations found in organoid cultures and matching tumor tissue obtained by targeted sequencing of 121 HGSOC-related genes confirms almost identical profile between parental tissue and *in vitro* long-term organoid culture. Color code indicates type of mutations which were detected.

B Representative Western blot showing loss or overexpression of p53 in individual organoid lines.

C Strong nuclear p53 signal in immunostainings of HGSOC organoids is indicative of a gain-of-function *TP53* mutation. Scale bars: 100 μm (tissue) and 50 μm (organoid).

D Multi-dimensional scaling (MDS) plot based on the gene expression profiles (microarrays) of three healthy FT and eight tumor tissue samples and their respective organoid cultures shows four clusters: normal FT tissue, normal FT organoids, cancer organoids, and cancer tissue.

E Box plots depicting overall constant level in normalized expression of major HGSOC marker genes between organoids and parental tissue. Data represent the median, quartiles, maximum, and minimum of the normalized expression from eight different donors.

F Heat map of differentially expressed genes between cancer and healthy tissue/organoids reveals up-regulation of several HGSOC biomarkers and reduction in FT differentiation markers in the cancer samples. Differential expression determined by single-color microarray for eight different patient samples was significant for all genes with *P* < 0.05 except for OVGP1 and TOP2A in organoids.

Source data are available online for this figure.

and Table S2), while the level of RB protein itself, which is phosphorylated by Cyclin E1 to promote G1/S progression, was not changed (Appendix Table S2). This indicates potential RB pathway disruption by increased Cyclin E1 levels. Amplification of CCNE1 gene is common in HGSOC (~ 20–30% of cases), but increased levels could also be a result of alternative signaling perturbations.

Together, these results demonstrate that the patient-derived OC organoid lines are valid *in vitro* models of the parental HGSOC tumors, resembling not only the tissue architecture but also the mutational profile and overall gene expression.

Stable triple knockdown of p53, PTEN, and RB in FT organoids

In the next step, we wanted to analyze at which stage of disease development the observed changes in niche factor requirements occur. This is a question of particular importance in HGSOC, where transformation appears to occur in the FT but cancers are very rarely detected at this site. To mimic the cellular events, like mutation of p53 and loss of PTEN, which characterize the early stages of malignant transformation, we used organoids from healthy FT donor epithelium. In contrast to previous *in vitro* tumorigenesis models, which were based on the transformation of immortalized primary FT monolayers (Jazaeri *et al*, 2011; Nakamura *et al*, 2018), organoids are genomically unaltered and have preserved epithelial polarity and integrity, thus ensuring mucosal homeostasis.

In order to model HGSOC development, shRNAs against p53, PTEN, and RB—major known tumor drivers of the disease—were introduced into healthy human FT epithelial cells from donor tissues obtained during surgeries for benign gynecological conditions. The shRNAs were delivered sequentially by retro- and lentiviral vectors into epithelial cells grown in 2D culture, selected by FACS (shPTEN-mCherry, shRB–GFP), and subsequently transferred to Matrigel to initiate organoid formation (Figs 3A and EV2A). Among the double-positive mCherry/GFP population (shPTEN, shRB), p53-depleted organoids were selected with puromycin. Successful knockdown of all three target genes was confirmed on RNA as well as protein level (Fig 3B). In total, seven triple knockdown (KD) cultures were successfully generated from different FT donor tissue confirming robustness of the methodology (Fig EV2D). In congruence with the downregulation of RB and PTEN protein, functional analysis of triple KD organoids revealed an increase in the expression of Cyclin E1 (Fig 3C) and elevated levels of activated phosphorylated Akt (pAkt), respectively (Fig EV2B). Functional disruption of p53 pathway was confirmed by resistance of organoids to the MDM2 inhibitor Nutlin-3A, which triggers apoptosis in p53 WT cells (Fig EV2C).

We next compared phenotypes of KD and WT organoids by confocal microscopy. We observed loss of cell shape and misalignment of the nuclei, indicative of changes in the maintenance of apicobasal polarity—although the organization of the monolayer remained intact and the lumen was preserved with a cystic growth of the organoids. Triple KD cells also showed a stronger signal for the DNA damage marker γH2AX, indicating an increased frequency of DNA double-strand breaks and thus suggesting genomic instability (Fig 3D). Notably, KD organoids had enlarged and polymorphic nuclei, which is one of the prominent morphological characteristics of HGSOC cells (Fig 3D). While all these phenotypic changes suggest that the knockdown of p53, PTEN, and RB in FT organoids is pro-carcinogenic, none is sufficient as bona fide evidence of malignancy. Indeed, KD cells remained competent to undergo differentiation into ciliated cells, which are thought to be the terminally differentiated cells of the FT (Fig 3E).

Rescue of KD organoid lines in ovarian cancer medium

Despite an initial growth advantage until the first passage after seeding, KD organoids cannot be maintained in long-term culture and undergo growth arrest after 4–8 passages, as shown by the growth curve in comparison with WT and vector control (Fig 4A and Appendix Fig S2A). While individual differences among different donor cultures were observed, the premature growth arrest of KD organoids was confirmed in 7/7 cases (Fig EV2D). This suggests that the KD organoids may undergo similar changes in stemness regulation as those observed in the HGSOC organoids.

Indeed, growing the organoids in ovarian cancer medium improved organoid formation efficiency and enabled long-term growth (Fig 4B). Importantly, long-term growth could only be rescued if OCM was added at passage 0/1, suggesting that inadequate niche conditions lead to irreversible loss of stemness. Phase-contrast images (Appendix Fig S2B) confirm that while individual organoids grow to a similar size, organoid numbers are lower at each passage in FTM, finally resulting in premature growth arrest. Western blot analysis of γH2AX and cleaved caspase-3, as well as PARP1, indicated that the growth-suppressive effect of Wnt3a did not result from direct cytotoxicity, as DNA damage and apoptosis were not reduced when organoids were grown in OCM (Fig 4C and Appendix Fig S2C). Single p53 or double p53/PTEN KD on the other
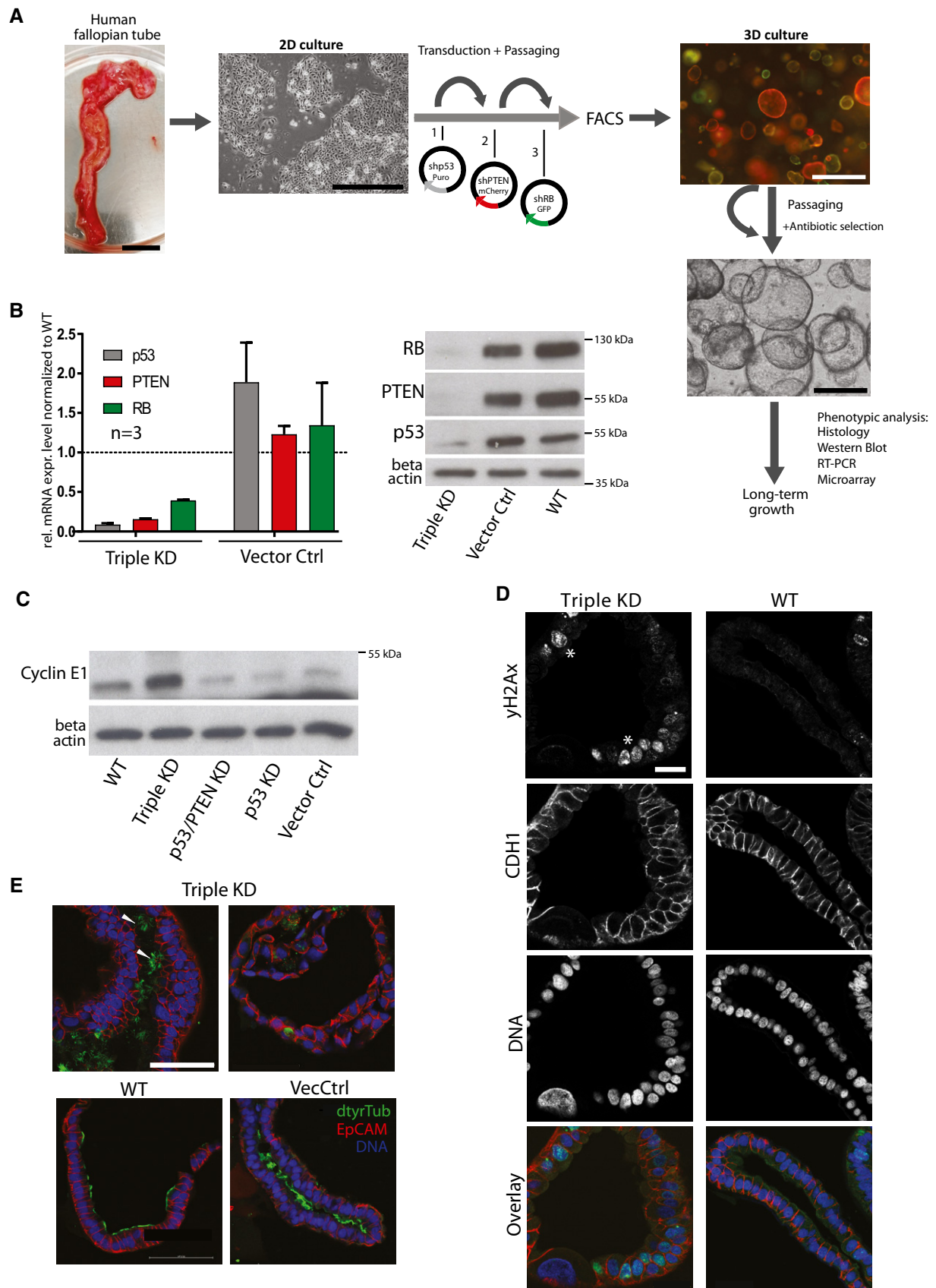
Figure 3.

Figure 3. Stable triple knockdowns of tumor suppressors p53, PTEN, and RB in healthy FT organoids.

A   Experimental approach for genetic manipulation of FT epithelial cells (FTECs). FTECs were sequentially transduced in 2D culture with replication-deficient viruses containing specific shRNAs and different selection markers. After sorting, cells were seeded in Matrigel for organoid formation. Scale bars: 2 cm (tissue), 200 μm (2D culture), and 500 μm (3D culture).

B   Confirmation of robust knockdowns of p53, PTEN, and RB in FT organoids on RNA and protein level. Relative mRNA levels were normalized to the WT mRNA level and are given as the mean ± SEM from three different donors. A representative Western blot from one donor is depicted. RNA and protein samples were taken at passage 1 or 2 of each organoid line. KD—knockdown, Vec Ctrl—vector control, WT—wild type.

C   Cyclin E1 overexpression as a downstream effect of RB knockdown was confirmed by Western blot analysis.

D   Confocal images of triple KD organoids reveal increased DNA damage (γH2AX, marked by asterisks), atypic nuclei (DRAQ5), and loss of apicobasal polarity. Scale bar: 20 μm.

E   Presence of ciliated cells (arrowheads), as revealed by immunostaining against detyrosinated Tubulin (dtyrTub) in triple KD organoids, proves capacity for terminal differentiation. Scale bar: 50 μm.

Source data are available online for this figure.

hand did not exhibit increased γH2AX levels, irrespective of the medium used, indicating that the enhanced DNA damage observed in triple KDs is the result of RB depletion.

In order to discover factors induced by culture in OCM that contribute to maintenance of stemness and longevity of the triple KD and HGSOC organoids, we performed global gene expression analysis. As expected, OCM medium devoid of Wnt3a and RSPO1 led to a reduction in the expression of Wnt target genes in both, triple KD and WT, organoids (Appendix Fig S2D). The microarray data also reveal that despite cell growth arrest of the KD organoids in FTM, they continue to show elevated expression of classical HGSOC markers, including FOXM1, TOP2A, CDKN2A, and WT1, albeit at lower levels than when grown in OCM (Fig 4D). This finding proves that knockdown of key tumor suppressor genes is sufficient to induce a degree of cellular transformation toward a cancer phenotype and supports the view that the FT epithelium is the tissue of origin of HGSOC.

However, a clear increase in the expression of genes related to stemness (CD133, MYCN, and SOX2) and a decrease in genes related to differentiation (PGR, OVGP1, and FOXJ1) were found in KD organoids grown in OCM vs. FTM (Fig 4E). While PGR and ESR1 are differentiation markers connected to hormone signaling, FOXJ1 is the major transcription factor required for ciliogenesis and thus development of multiciliated cells, presumed to be the terminally differentiated cell type in the FT mucosa. The downregulation of FOXJ1 compared to the vector control was validated by qPCR for organoids from two patients (Fig 4F). In addition, quantification of immunolabeling against detyrosinated tubulin (Fig 4G) in three independent organoid lines confirmed a lack of multiciliated cells in the triple KD organoids grown in OCM, but not in FTM. Since FT mucosa renewal is driven by the differentiation of bipotent progenitors (Kessler *et al*, 2015; Ghosh *et al*, 2017), the absence of ciliated cells is suggestive of a shift toward the secretory phenotype. Notably, an outgrowth of secretory cells is thought to be a critical step in the development of HGSOC from FT epithelium. Our findings indicate that this process can be triggered *in vitro* by p53/PTEN/RB depletion, provided that canonical Wnt pathway activation is reduced.

Wnt-free medium supports stemness of HGSOC and KD organoids

Next, we wanted to confirm independently that Wnt-free medium increases stemness of KD organoids. FACS analysis of the bona fide OC stem cell marker CD133 (Kryczek *et al*, 2012), which is expressed on the cell surface, revealed that the number of positive cells in triple KD organoids increased when cultured in OCM vs. FTM (Fig 5A and Appendix Fig S3A). In vector ctrl and WT cells, by contrast, the number of CD133$^+$ cells was lower in OCM, consistent with FTM providing more optimal conditions for the preservation of stemness in healthy epithelial cells. Loss of stemness coincides with a reduction in growth potential as quantified by a luciferase-based assay determining the number of live cells after two passages of parallel cultivation in the different media (Fig 5B). This confirms that the presence of Wnt agonists in the environment hampers the growth of p53/PTEN/RB KD organoids by repressing stemness—indicative of a substantial change in stemness regulation.

To substantiate these results, we analyzed the direct effect of Wnt3a/RSPO1 supplementation on patient-derived HGSOC organoid growth and CD133 surface expression. Differential treatment of cancer organoids over 2 passages clearly showed that addition of these Wnt agonists to OCM resulted in a highly significant ($P < 0.001$) inhibition of organoid growth, an effect confirmed for all five OC organoid lines tested (Fig 5C). Interestingly, the inhibitory effect of Noggin on already established cultures was mild, but significant, confirming that BMP pathway activity is beneficial for growth but not as essential as for initial organoid formation. However, addition of Noggin to mature organoid lines had no effect on the number of CD133$^+$ cells, while the presence of Wnt3a/RSPO1 reduced CD133$^+$ numbers significantly (Fig 5D and Appendix Fig S3B), suggesting that the negative influence of canonical Wnt pathway activation on HGSOC organoid growth is potentially connected to the regulation of CD133 surface expression.

As Wnt3a supplementation relies on the addition of conditioned medium from a Wnt-producing cell line, we next wanted to confirm that its effect was specific to the presence of Wnt. Indeed, Wnt-conditioned medium strongly upregulated the established Wnt target gene AXIN2 (Appendix Fig S3C). In addition, medium conditioned by the parental cell line without the Wnt-producing vector (CM) did not negatively affect organoid growth (Fig 5E).

Overall, it can be concluded that the presence of Wnt ligands, which induce a signature of canonical Wnt target gene expression in KD and HGSOC organoids, results in a striking decrease in stemness and growth capacity in these cultures.

MYCN and Wnt inhibitors are upregulated in HGSOC and KD FT organoids

The data from HGSOC organoids provide strong evidence that the mechanisms by which growth of cancer organoid stem cells is
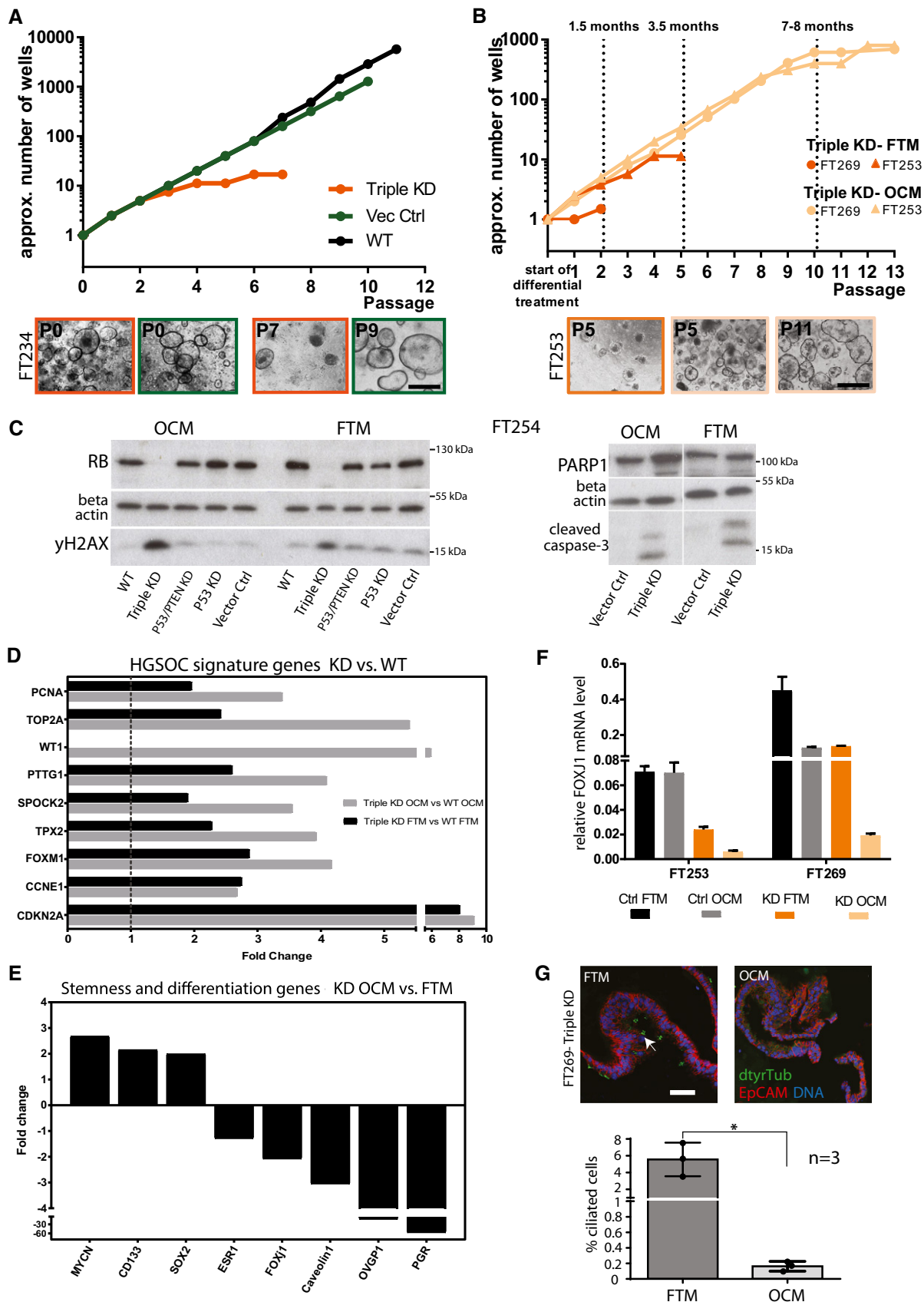
Figure 4.

Figure 4. Triple KD organoids show improved growth in ovarian cancer medium.

A   In long-term 3D culture, triple KD organoids show loss of growth capacity and premature growth arrest compared to the controls as indicated by the representative growth curves of FT234. Scale bar: 500 µm.

B   Growth curves and phase-contrast images of triple KD organoids grown in OCM compared to FTM reveal successful rescue of long-term growth capacity. Scale bar: 500 µm.

C   Levels of DNA damage (γH2AX) and apoptosis (cleaved caspase-3, PARP1) do not differ among the different media as shown by representative Western blots comparing triple KD organoids and their controls.

D   Triple KD (p53/PTEN/RB) organoids are characterized by a HGSOC gene expression signature as revealed by microarray analysis comparing WT and KD organoids grown in either OCM or FTM. Differential expression determined by dual-color microarray for two biological replicates was significant for all genes with $P < 0.00005$.

E   Differential expression of stemness- and differentiation-related genes of triple KD organoids grown in OCM vs. FTM. Fold changes were derived from microarray data and indicate an increase in stemness (CD133, SOX2, MYCN) and a drop in differentiation (OVGP1, PGR, FOXJ1) under OCM conditions. Differential expression determined by dual-color microarray for two biological replicates was significant for all genes with $P < 0.05$.

F   FOXJ1 expression determined by qPCR was significantly diminished in triple KD organoids grown in OCM compared to FTM, suggesting a decrease in differentiation capacity. Data represent the mean ± SEM from technical triplicates for two independent knockdown cultures.

G   Proportion of ciliated cells (detyrosinated tubulin; dtyrTub) is significantly reduced in KD organoids under OCM growth conditions, confirming inhibition of differentiation as illustrated by confocal images (Scale bar: 50 µm). The quantification plot depicts the mean ± SEM from three independent biological replicates, based on quantification of the average number of ciliated cells per counted nuclei. 1,000 cells were counted per individual experiment. *$P < 0.05$, two-sided Student's t-test.

Source data are available online for this figure.

maintained are altered from those in the healthy epithelium, and our experiments with KD organoids further show that depletion of only three tumor driver genes can recapitulate this effect. To get a better insight into putative candidate genes that could contribute to the maintenance of stemness in cancer organoids, we compared microarray data of healthy FT epithelium and HGSOC tissue as well as patient-derived cancer and KD organoids grown in the ovarian cancer minimal medium (OCM) vs. the fallopian tube medium (FTM) (Fig 6A). The proto-oncogene MYCN was uniformly upregulated in cancer tissue, as well as triple KD organoids cultured in OCM, suggesting that it may play a role in driving stemness and cancer growth in HGSOC. qPCR confirmed MYCN expression to be significantly higher in cancer organoids compared to FT organoids (Fig 6B, left panel). In addition, the expression levels of MYCN relative to GAPDH were validated by qPCR in three independent biological replicates of triple KD organoids cultured in OCM vs. FTM (Fig 6B, right panel).

In line with our finding that reduced canonical Wnt signaling supports the growth of cancer organoids, the gene expression data revealed enhanced expression of the Wnt inhibitors KREMEN2 and DKK3 (Mao *et al*, 2002; Yue *et al*, 2008) in both triple KD and OC organoids (Fig 6A). While KREMEN2 regulation appears to be driven by changes in the genetic background, DKK3 expression seems to be induced by Wnt-free medium. Therefore, it appears that the altered paracrine signaling environment further promotes inhibition of canonical Wnt signaling. Interestingly, downregulation of p53/PTEN/RB in FT organoids caused a decrease in Wnt target gene expression even in the presence of Wnt3a and RSPO1 (Fig 6C), while culture in Wnt-free medium leads to a further strong reduction in LEF1 and TCF transcripts down to the detection limit of the microarray (Appendix Table S3). The expression of Wnt inhibitors and the reduced Wnt signaling induced by tumor suppressor KD are in agreement with our hypothesis that Wnt pathway suppression is required for HGSOC growth, which can be achieved by different molecular mechanisms—cell autonomous and/or by changes in the niche environment. Interestingly, HGSOC organoids expressed increased levels of differentiation markers when exposed to Wnt3a/RSPO1. In line with the microarray results and data from the triple KD organoids, qPCR confirmed increased expression of the

ciliogenesis factor FOXJ1 in cancer organoids cultured in the presence of Wnt3a/RSPO1 (Fig 6D). Based on this, we postulate a two-step process of HGSOC development in which changes in the niche environment are a necessary step that drives dedifferentiation and maintains stemness in cells bearing tumorigenic mutations.

Discussion

Our understanding of the cellular mechanisms that underlie the development of HGSOC in the FT and its spread to the ovaries and beyond remains rudimentary and represents a major obstacle to advances in diagnosis and therapy. Although some properties of cancer stem cells in HGSOC have been described (McLean *et al*, 2011; Choi *et al*, 2015; Lupia & Cavallaro, 2017), there is no knowledge about the intrinsic mechanisms that drive tumor growth and mediate recurrent disease. As patients frequently receive neoadjuvant chemotherapy prior to debulking surgery, such tumor samples are likely to already show secondary biological alterations. This study thus provides systematic insight into the biology of HGSOC organoids derived directly from primary debulking surgery samples, which reflect the biology of the initial cancer tissue.

In contrast to the healthy FT epithelium (Kessler *et al*, 2015), we find that HGSOC cancer organoids require a low-Wnt signaling environment but an active BMP signaling axis. Wnt independence was previously observed in other cancers such as pancreas and colon (Fujii *et al*, 2016; Seino *et al*, 2018) and positively correlates with the clinical progression. However, in contrast to organoids from other cancers, e.g., metastatic pancreatic cancer, which do not require Wnt but do grow in Wnt/RSPO/Noggin medium, exogenous supplementation of Wnt3a actually prevented formation and growth of all HGSOC cancer organoids. Recently, Kopper *et al* (2019) also reported the use of Wnt-free medium for the generation of HGSOC organoids but attributed negative effect of Wnt to the potential contaminating presence of serum. Here, we clearly show that lack of exogenous Wnt signal activation is in fact a requirement for maintaining stemness and preventing differentiation in HGSOC organoids and that pro-cancerous mutations by themselves are therefore likely not sufficient to drive transformation of healthy
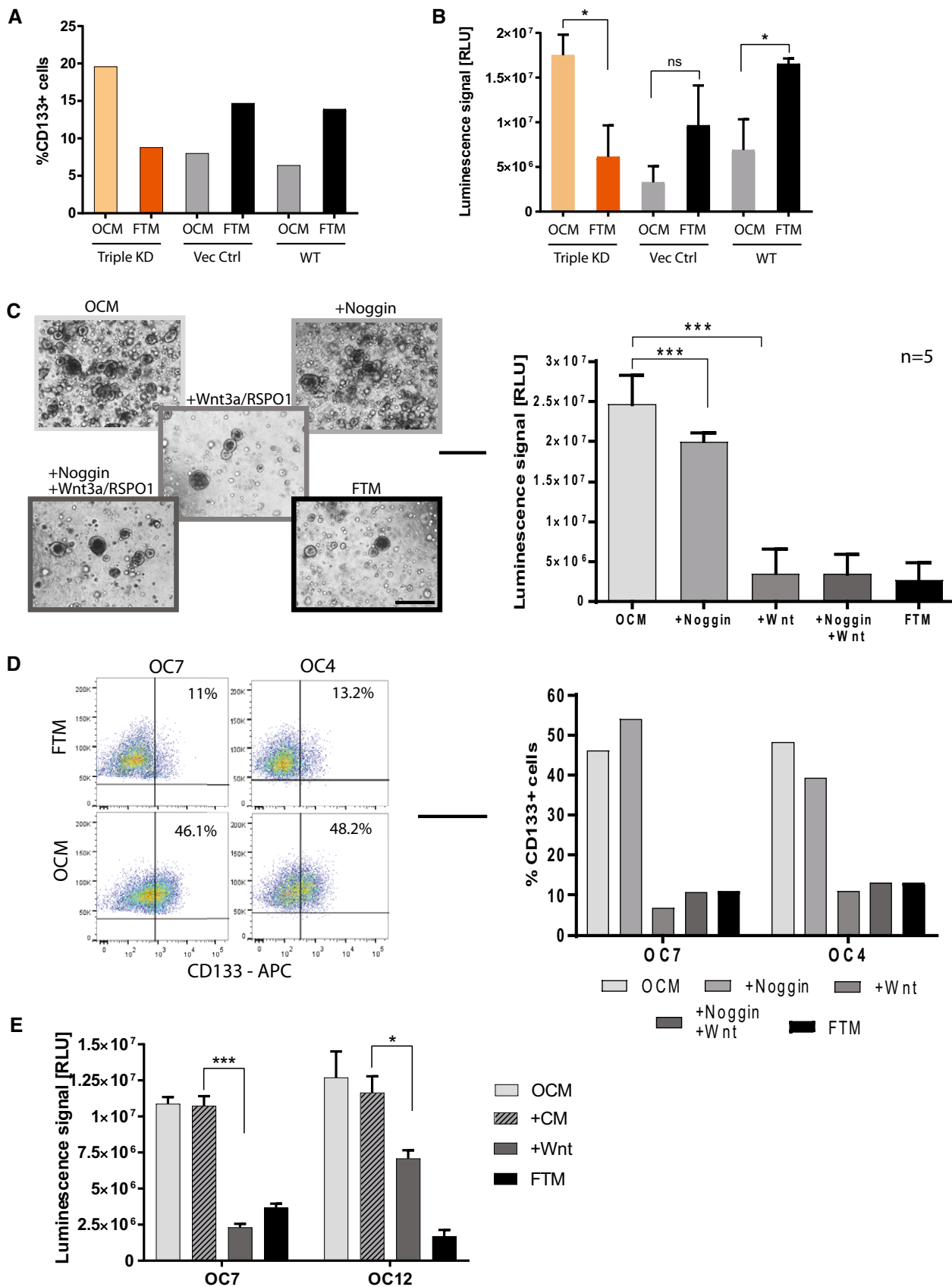
Figure 5.

Figure 5. Wnt depletion supports preservation of stemness in HGSOC organoids.

A   The proportion of CD133^{+} cells was determined by FACS analysis after growing triple KD and control cells in FTM vs. OCM for two passages. The graph is representative of two biological replicates.

B   Growth capacity increases when KD organoids are grown in OCM medium as shown by difference in total viable cell number (representative graph of three independent experiments). The luminescent cell viability assay was performed in triplicate, and the bar plot depicts the mean ± SEM. *$P < 0.05$, two-sided Student's *t*-test; KD—knockdown, Vec Ctrl—vector control, WT—wild type.

C   Phase-contrast images of cancer organoids which entered growth arrest upon treatment with Wnt agonists (Wnt3a/RSPO1) over two passages (Scale bar: 500 μm). Differences in cell number were confirmed by the respective cell viability assays (performed in technical triplicates). Data represent the mean ± SEM for five different OC organoid lines ($n = 5$). ***$P < 0.001$, two-sided Student's *t*-test.

D   The number of CD133^{+} cells determined by FACS for OC7 and OC4 organoids grown in different media with or without Wnt3a/RSPO1 and with or without Noggin over two passages confirms a sharp drop in stemness in the presence of Wnt agonists.

E   Addition of conditioned medium collected from the parental Wnt3a cell line did not suppress growth of cancer organoids, proving that the growth inhibitory effect is due to the presence of Wnt agonists. The bar plot represents the mean ± SEM of triplicates performed with a luminescent cell viability assay. *$P < 0.05$, ***$P < 0.001$, two-sided Student's *t*-test.

epithelium. Importantly, activation of Wnt pathway through action of the GSK3-β inhibitor CHIR also inhibits organoid growth, which independently confirms functional relationship between low-Wnt signal and maintenance of HGSOC growth potential *in vitro*. This provides mechanistic experimental validation of findings from a large GWAS study that identified genomic variants of the Wnt pathways agonist Wnt4 and RSPO1 loci to be associated with increased susceptibility for epithelial ovarian cancer development, and showed decreased expression of Wnt4 in the cancer tissue (Kuchenbaecker *et al*, 2015). Although we used Wnt3a in our experiments, the extensive functional redundancy among the Wnt family members suggests that Wnt4 stimulation would have a similar effect.

Notably, we also clearly demonstrate that active BMP signaling is an important factor for the formation of cancer organoids (13/15 lines could only be initiated without Noggin in the medium), and for long-term growth. As Noggin was a standard medium component in previous studies (Hill *et al*, 2018; Kopper *et al*, 2019), this potentially explains the reported difficulties with long-term maintenance. Thus, it is tempting to speculate that the overall environment in the FT epithelium (with presumably high-Wnt signaling) represses cancer outgrowth and promotes escape of (pre-)malignant cells to more distant sites, like the surface of the ovaries and peritoneum. Interestingly, even the formation of the two organoid cultures that benefited from the presence of RSPO1 (Fig 1) could be efficiently prevented by addition of Wnt3a and Noggin, suggesting high sensitivity of the HGSOC organoids to elevated Wnt signaling. Nevertheless, these cases show that the heterogeneity of this disease warrants routine testing of two different media during the establishment of fresh cultures: OCM and OCM + RSPO1 and FGF.

Our analysis of HGSOC and KD organoids clearly demonstrates that a high-Wnt environment leads to the downregulation of stemness genes and the up-regulation of differentiation genes. Mouse lineage tracing data previously showed that active Wnt signaling is required for both renewal of Pax8 secretory cells and their differentiation to ciliated cells (Ghosh *et al*, 2017). Our data strongly suggest that the regulation of these processes becomes separated during carcinogenesis. While Wnt stimulation still induces differentiation and ciliogenesis in cancer organoids, it inhibits their longevity and expansion capacity. The same effect is observed in triple KD organoids, indicating that depletion of key tumor driver proteins is sufficient to induce these alterations in stem cell regulation. Yet, despite the change in growth requirements, the prominent occurrence of

nuclear atypia, increase in DNA damage, and changes in epithelial organization, triple KD organoids maintained key elements of epithelial polarity. Therefore, it appears they have not completed the process of transformation and that additional changes are needed for malignancy to develop. This is also in line with the observation that growth rescue in OCM medium was incomplete. Unlike the stable long-term expansion of HGSOC organoids, which were routinely cultured for over 1 year without changes in growth dynamics, the lifespan of KD organoids in OCM was limited to 7–8 months.

Our data illustrate the critical importance of the model system when studying processes of cell transformation *in vitro*. Several previous studies on the putative role of the FT as the tissue of origin of HGSOC showed the transformation potential of human FT epithelial cells in 2D cell culture by overexpression of different oncogenes (h-RAS, c-MYC) followed by xenograft transplantation (Jazaeri *et al*, 2011; Karst *et al*, 2011). We show that robust regulatory mechanisms in the intact epithelium prevent the breakdown of the epithelial organization despite functional inactivation of the key HGSOC drivers p53, PTEN, and RB. Breakdown of apicobasal polarity is an important step in the emergence of many cancers, as it precedes EMT and thus facilitates cancer progression (Huber *et al*, 2005; Ozdamar *et al*, 2005). While our microarray data revealed important similarities in gene expression profile between KD FT organoids and mature cancer organoids, further studies are needed to elucidate the exact mechanism of cancer stem cell maintenance in HGSOC. MYCN, which in the absence of Wnt was ubiquitously upregulated in all HGSOC and KD FT organoids in our study, was previously implicated as a driver of stemness in aggressive glioblastoma (Yang *et al*, 2017b). The high degree of consistency in MYCN regulation in KD FT and HGSOC organoids from independent donor samples warrants further studies to investigate its potential role as a stemness marker in HGSOC. Also, while we show that surface expression of CD133 correlates with *in vitro* growth capacity of HGSOC organoids, the exact functional relationship between stemness regulation in the organoid culture and other previously described ovarian cancer stem cell markers CD117, ALDH1 and CD24 (Gao *et al*, 2010; Kryczek *et al*, 2012; Yang *et al*, 2017a) is yet to be tested.

Our data strongly suggest the existence of signaling cross-talk between stemness maintenance in FT epithelium and the major drivers of cellular transformation in HGSOC—p53, PTEN, and RB. Although our KD FT organoids modeled conditions where p53 is depleted, the patient-derived HGSOC lines included both loss-of-function p53 mutations and frequent gain-of-function alleles. No
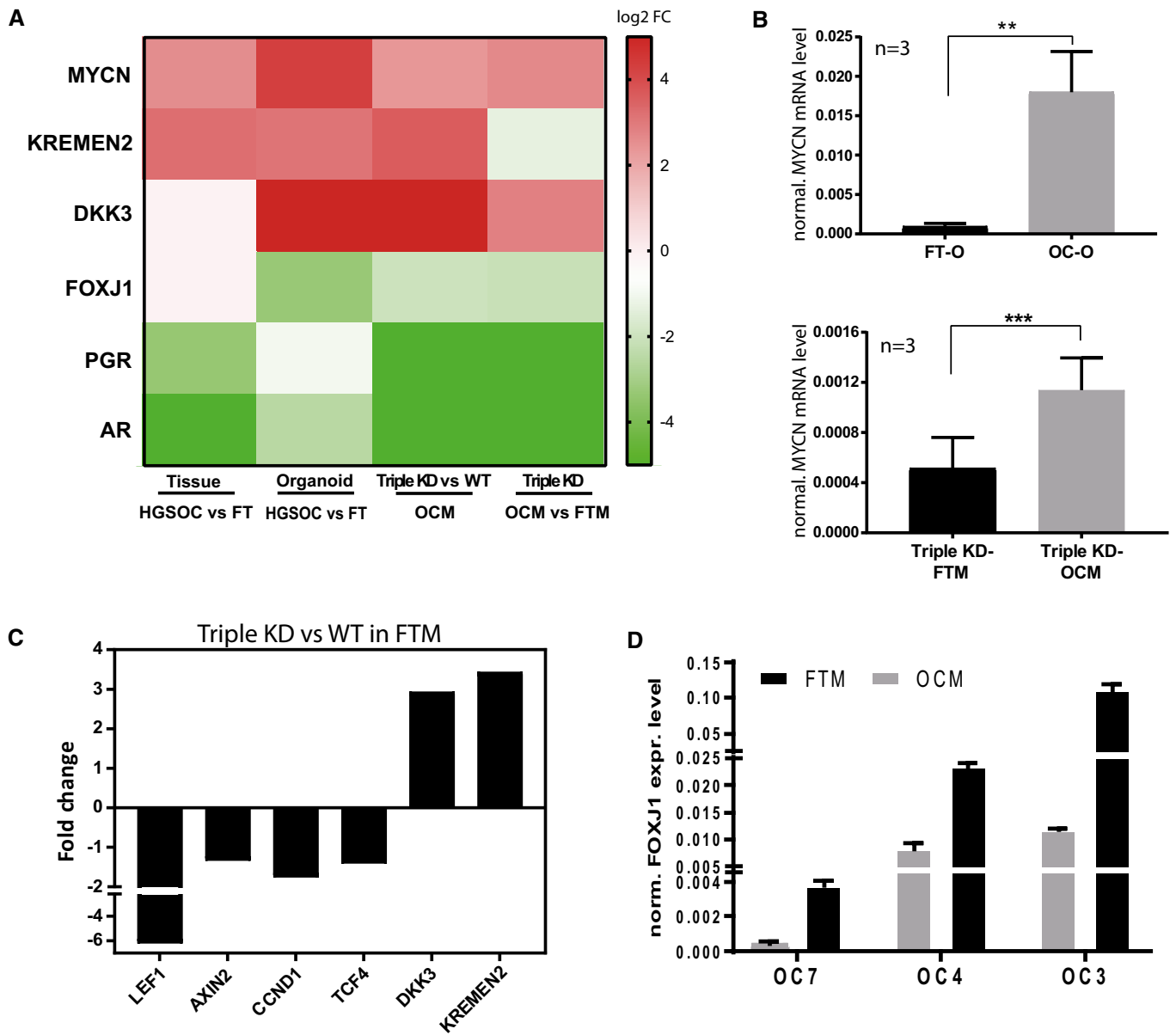
Figure 6. Unifying induction of MYCN and Wnt inhibitors in HGSOC and KD samples.

A   Comparative analysis of microarray data revealed consistent up-regulation of MYCN and the canonical Wnt inhibitors KREMEN2 and DKK3 as well as down-regulation of differentiation marker FOXJ1, AR, and PGR in HGSOC cancer organoids as well as triple KD FT organoids. Differential expression was determined either by single-color microarray for the cancer samples (eight replicates) or by dual-color microarray for the knockdowns (two replicates) and is significant for all genes with $P < 0.05$.

B   Transcriptional induction of MYCN is confirmed by qPCR for three patients between cancer organoids and normal FT organoids as well as triple KD organoids grown in OCM vs. FTM conditions. Depicted is the mean $\pm$ SEM of the normalized MYCN mRNA expression level of three biological replicates ($n = 3$). **$P < 0.01$, ***$P < 0.001$, two-sided Student's *t*-test.

C   Microarray data revealed that the expression levels of Wnt target genes are downregulated in triple KD compared to WT control FT organoids. Differential expression determined by dual-color microarray for two biological replicates was significant for all genes with $P \leq 0.005$.

D   FOXJ1 expression was upregulated in HGSOC organoids in FTM compared to OCM as shown by qPCR analysis of three different patient samples. Data represent the mean $\pm$ SEM of technical triplicates.

difference in growth factor requirements was detected in relation to the type of p53 mutation.

The stability of patient-derived HGSOC organoid lines cultured using our method makes it potentially suitable for translational biomedical research. Preliminary tests with carboplatin showed

individual differences in drug response of organoids from different patients. However, to define to which extent organoids are predictive of *in vivo* patient responses, more comprehensive *in vitro* drug testing studies in correlation with long-term clinical outcome are needed. In order to identify how stem cells respond to cancer

therapy, which is of critical importance for the development of new treatment approaches, paired organoid cultures could be generated from primary disease and after recurrence in the same patients.

It is possible that including other cell types in the organoid model, such as stromal and immune cells, could further advance its capacity to generate data which are predictive of clinical responses in patients (Neal *et al*, 2018).

Overall, this study provides important insight into fundamental biological processes of HGSOC development. We show that functional inactivation of key tumor drivers fails to induce a direct growth advantage of the altered cells in the absence of appropriate changes in the stem cell niche environment. The existence of such a two-component mechanism opens up important new questions for understanding the etiology of HGSOC—in particular which cellular and physiological mechanisms in the tissue surrounding the FT epithelium are responsible for the critical changes in paracrine signaling that favor the outgrowth of mutated cells. In this context, the regulatory role of the neighboring ovary could further be of pivotal relevance, particularly in light of epidemiological data showing a strong correlation between inflammatory processes associated with ovulation and the risk for HGSOC development.

Materials and Methods

Reagents and Tools table

Reagent/Resource	Reference or source	Identifier or catalog number
Experimental models		
HEK-293 cells (*Homo sapiens*)	ATCC	CRL-11268
L cells	ATCC	CRL-2648
L Wnt-3a	ATCC Willert *et al* (2003)	CRL-2647
293T HA Rspo1-Fc	R&D Farin *et al* (2012)	3710-001-01
293T WntR	This study	
Recombinant DNA		
psPAX2	Addgene	12260
pMD2.G	Addgene	12259
pLVTHM-GFP	Addgene	12247
pLVTHM-GFP-shLuciferase	This study	Appendix Table S4
pLVTHM-mCherry-shLuciferase	This study	Appendix Table S4
pLVTHM-mCherry-shPTEN	This study	Appendix Table S4
pLVTHM-GFP-shRB	This study	Appendix Table S4
pSUPER.retro	Addgene	3926
pSUPER.retro.p53	Alexander Löwer (Brummelkamp *et al*, 2002)	Appendix Table S4
retroviral packaging plasmid	Alexander Löwer (Brummelkamp *et al*, 2002)	
retroviral envelope plasmid	Alexander Löwer (Brummelkamp *et al*, 2002)	
Antibodies		
Rabbit anti-BRCA1, WB (1:200)	Santa Cruz	sc-642
Mouse anti-cyclin E1 (HE12), WB (1:1,000)	Cell Signaling	4129
Rabbit anti-cleaved caspase-3 (Asp175), WB (1:1,000)	Cell Signaling	9661
Rabbit anti-detyrosinated α-tubulin, IHC (1:100)	Abcam	ab48389
Mouse anti-E-Cadherin, IHC (1:100)	BD Biosciences	610181
Mouse anti-EpCAM (VU1D9), IHC (1:100)	Cell signaling	2929S
Mouse anti-EpCAM (VU1D9), IHC (1:100)	Thermo Scientific	MA1-10195

Reagents and Tools table (continued)

Reagent/Resource	Reference or source	Identifier or catalog number
Mouse anti-p16 (16P04), IHC (1:600)	NeoMarkers	
Mouse anti-p53 (1C12), IHC (1:2,000)	Cell Signaling	2524
Mouse anti-p53 (DO-1), WB (1:500)	Santa Cruz	sc-126
Mouse anti-p53 (DO-7), (1:50)	Dako	M7001
Mouse anti-PARP, WB (1:2,000)	Cell Signaling	9542
Rabbit anti-Pax8, IHC (1:50)	Proteintech	10336-1-AP
Mouse anti-Pax8 (MRQ-50), IHC (1:100)	Sigma	363M-1
Rabbit anti-phospho γH2AX (Ser139), WB (1:1,000), IHC (1:400)	Cell signaling	9718
Rabbit anti-PTEN, WB (1:1,000)	Cell Signaling	9552
Mouse anti-Rb (4H1), WB (1:2,000)	Cell Signaling	9309
Donkey anti-mouse IgG (H+L) Alexa-Fluor® 488, IHC (1:100)	Dianova	715-454-151
Donkey anti-rabbit IgG (H+L) Alexa-Fluor® 488, IHC (1:100)	Dianova	715-545-152
Donkey anti-mouse IgG (H+L) Cy3, IHC (1:100)	Dianova	715-166-140
Donkey anti-rabbit IgG (H+L) Cy3, IHC (1:100)	Dianova	711-165-152
Sheep anti-mouse IgG HRP Linked Whole Ab, IHC (1:3,000)	GE Healthcare	NA931
Donkey anti-rabbit IgG HRP Linked Whole Ab, IHC (1:3,000)	GE Healthcare	NA934
Mouse anti-CD133/1 (AC133)—APC, FC (1:100)	Miltenyi Biotec	130−090−826
Anti-mouse IgG1 Isotype control APC, FC (1:100)	Miltenyi Biotec	130-098-846
Oligonucleotides		
qPCR primers	This study	Appendix Table S5
Chemicals, enzymes and other reagents		
Advanced DMEM/F12 (ADF)	Gibco	12634
B27 supplement (50×)	Gibco	17504044
BMP2 (human)	Gibco	PHC7146
Carboplatin	Merck	216100
EGF (human)	Gibco	PHC7146
Fetal calf serum (FCS)	Biochrom	S0115
FGF-10 (human)	PeproTech	100-26-B
GlutaMax (100×)	Gibco	35050-038
HEPES (1 M)	Gibco	15630-056
L-Glutamine	Gibco	25030-024
N2 supplement (100×)	Gibco	17502048
Na-pyruvate	Sigma-Aldrich	S8636
Nicotinamid	Sigma-Aldrich	N0636
Noggin (human)	PeproTech	120-10C
Nutlin-3a	Sigma-Aldrich	N6287
Penicillin/Streptomycin	Gibco	15140-122
Puromycin	Gibco	A11138-03

Reagents and Tools table (continued)

Reagent/Resource	Reference or source	Identifier or catalog number
Y-27632 dihydrochloride monohydrate (ROCK inhibitor)	Sigma-Aldrich/Chemdea	Y0503/CD0141
Rspo-1	In-house production	
SB431542 (TGF-β inhibitor)	Calbiochem	616454
Wnt3a	In-house production	
CHIR99021	Sigma	SML1046
Collagenase type I	Sigma	C5138
Collagenase type II	Biochrom	C2-28
Cryo-SFM	PromoCell	C-29910
DMEM (high glucose, NEAA, no glutamine)	Gibco	10938-025
Dulbecco's phosphate buffered saline (DPBS)	Gibco	14190-169
Matrigel™ (basement membrane matrix, Growth factor reduced)	Corning	356231
TrypLE™ Express	Gibco	12605-028
Zeocin	Gibco	R250-01
Acrylamid/Bisacrylamid	Roth	3029.1
Amersham Hyperfilm ECL	GE Healthcare Life Sciences	28906835
Bovine serum albumin (BSA)	Biomol	01400.1
Carboplatin	Merck	216100
DRAQ5 (5 mM)	Thermo Scientific	65-0880-96
Eosin Y solution	Roth	7089.3
FuGENE® 6	Promega	E2691
HistoBond® microscope slides	Marienfeld	0810000
Mayer's hematoxylin solution	Roth	T865.1
Milk powder	AppliChem	A0830,1000
Mowiol® 4-88	Sigma	81381
Opti-MEM™	Thermo Scientific	31985070
Paraformaldehyde (PFA)	Sigma-Aldrich	4441244
Propidium iodide	Thermo Scientific Invitrogen™	P3566
Polybrene	Sigma-Aldrich	H9268
PVDF membrane Polyscreen®	PerkinElmer™	NEF100200
Roti®-Histokitt	Roth	6638.2
TEMED	Roth	8142.1
Target retrieval solution (10×)	Dako	S1699
TRIzol® reagent	Invitrogen™	15596026
Western Lightning Chemiluminescence Reagents	PerkinElmer	NEL103001EA
Software		
Adobe Creative Cloud	https://www.adobe.com/gr_en/creativecloud/desktop-app.html	
Corel Draw X7	https://www.coreldraw.com/en/pages/coreldraw-x7/	
Clone Manager	https://www.scied.com/pr_cmbas.htm	

Reagents and Tools table (continued)

Reagent/Resource	Reference or source	Identifier or catalog number
FlowJo vX.0.6	https://www.flowjo.com/solutions/flowjo	
ImageJ1.47v	https://imagej.nih.gov/ij/index.html	
GraphPad Prism® 7.03	https://www.graphpad.com	
RBioconductor	https://www.bioconductor.org/	
RStudio	https://rstudio.com/	
LAS AF software	https://www.leica-microsystems.com/products/microscope-software/details/product/leica-las-x-ls/	
Other		
ultraView Universal DAB detection kit	Ventana	760-500
CellTiter-Glo® 3D Cell Viability Assay	Promega	G9681
Two-color Quick-Amp Labeling Kit	Agilent Technologies	5190-0444
One-color Low Input Quick Amp Kit	Agilent Technologies	5190-2305
4 × 44K whole human genome microarray	Agilent Technologies	014850
8 × 60K human custom microarray	Agilent Technologies	048908
Lenti-X™ concentrator	Clontech	631232
Plasmid Midi Kit	QIAGEN	12143
RNeasy Mini Kit	QIAGEN	74104
AllPrep DNA/RNA Mini Kit	QIAGEN	80204
Quick Ligation Kit	NEB	M2200
Qubit™ dsDNA HS Assay Kit	Thermo Fisher	Q32851
AB Power SYBR® Green RNA-to-CT™ 1-Step Kit	Thermo Fisher	4389986
Ventana Benchmark XT Autostainer instrument	Ventana Medical Systems	
SP-8 confocal microscope	Leica	
TCS SP-E confocal microscope	Leica	
Western Blot system	Bio-Rad	
NanoDrop 1000 UV/Vis spectrophotometer	Kisker	
Agilent 2100 Bioanalyzer	Agilent Technologies	
G2565CA high-resolution laser microarray scanner	Agilent Technologies	
Paraffin Rotation Microtome HM315	Microm	
Tissue processor TP1020	Leica	
Megacentrifuge 2.0 R	Heraeus Instruments	
StepOnePlus™ Real-Time PCR System	Applied Biosystems	
Sorvall centrifuge and rotor SS34	Sorvall	
Master Cycler Gene Amp® PCR System 9700	Thermo Fisher	
FACSCanto™ II	BD Biosciences	
LSRFortessa™	BD Biosciences	
FACSAria II	BD Biosciences	

Methods and Protocols

Procurement of human material

Approval for the preparation and experimental usage of the primary material was given by the Ethics Commission of the Charité, Berlin (EA1/002/07), and informed consent was obtained from every patient. Human fallopian tube (FT) samples were provided by the Auguste-Viktoria-Klinikum Berlin, Department of Gynecology and Obstetrics, while ovarian cancer samples were received from the Department of Gynecology, Charité University Hospital, Campus Virchow Clinic.

Tissue processing and organoid culture of FT samples

Only anatomically normal fallopian tubes removed by standard surgical procedures for benign gynecological disease were used for cell isolation. The tubes were transported and dissected within 2–3 h of removal. Of each FT sample, one piece was saved for RNA/DNA preparation.

1   After washing with DPBS and longitudinal opening of the FT with scissors, the tissue was incubated in collagenase I (Sigma) for 45–60 min at 37°C for enzymatic detachment of epithelial progenitors.
2   Subsequently, the mucosal cells were scraped off the muscularis with a scalpel, resuspended in the enzyme solution, mixed with one volume of ADF supplemented with 1× GlutaMax and 10 mM HEPES (ADF + +), and pelleted by centrifugation (7 min, $300 \times g$).
3   Cells were seeded in 2D culture with ADF + + supplemented with 5% FCS, Pen/Strep, 10 ng/ml hEGF, and 9 μM ROCK inhibitor (2D medium) for up to 1 week before transfer into Matrigel™ for organoid formation.

The FT organoids were cultured as described in Kessler *et al* (2015).

1   To initiate organoid growth, approximately 30,000 cells, obtained from 2D culture by incubation with the TrypLE™ enzyme mixture (10 min, 37°C), were seeded in one 50 μl drop of Matrigel™ per well of an uncoated 24-well plate.
2   The plate was placed in a humidified incubator at 37°C for 30 min to allow the Matrigel™ to polymerize before being overlaid with 500 μl of a growth factor cocktail stimulating different paracrine pathways including EGF and Wnt signaling. The detailed composition of the fallopian tube organoid medium (FTM) is given in Table EV2.
3   Medium was changed every 3–4 days, and organoids were expanded every 2–3 weeks at a rate of 1:2–1:3.
4   For expansion, organoids were released from Matrigel™, washed with ADF + +, taken up in pre-warmed TrypLE™, and incubated for 7–10 min at 37°C for enzymatic digestion.
5   Subsequently, organoids were vortexed three times for 3 s, washed with ADF + +, and pelleted by centrifugation (5 min at $300 \times g$).
6   Finally, the shredded organoids were resuspended in fresh Matrigel™ and seeded into pre-warmed cell culture plates before FTM was added to the organoids.

Tissue processing and organoid culture of ovarian cancer samples

Cancer samples, surgically removed from patients with a preliminary diagnosis of HGSOC, were retrieved from tumors of specified sites within the abdominal cavity. The tumor material was transported and processed within few hours after surgery, and each sample was divided into three pieces for cell preparation, tissue fixation, and RNA/DNA isolation.

1   For isolation of HGSOC progenitors, the tissue pieces were washed with DPBS, minced with a scalpel into very small pieces, transferred to a 50-ml falcon tube, and incubated in a 1:1 mixture of collagenase I and collagenase II (Sigma) for around 60 min at 37°C on a shaker.
2   To further separate the cells mechanically, the enzyme-tissue mixture was vortexed two times for 10 s. Next, one volume of ADF + + was added and the cell suspension was centrifuged (5 min, $300 \times g$, 4°C).
3   The cell pellet was resuspended in ADF + +, and cells were counted using a Neubauer chamber.
4   After initial isolation from the tumor tissue, ovarian cancer cells were seeded in Matrigel™ at a concentration of approx. 30,000 cells/50 μl.
5   In order to determine growth requirements for HGSOC organoids, isolates were seeded in parallel in different media compositions to test requirement for selected paracrine niche factors including BMP and Wnt pathway (Table EV3). The optimal growth medium for each patient-derived HGSOC organoid line is listed in Table EV3.
6   Upon proper organoid maturation and growth under specified conditions, they were split at a ratio of 1:3 every 2–3 weeks.
7   For passaging, they were released from Matrigel™ using ice-cold ADF + +, centrifuged at $300 \times g$ for 5 min, and resuspended in 500 μl pre-warmed TrypLE™ per well. Enzymatic digestion was carried out for 7 min at 37°C.
8   Afterward, the organoid suspension was vortexed three times for 3 s, mixed with cold ADF + + at a ratio of 1:1, and centrifuged at $300 \times g$ for 5 min.
9   Next, the supernatant was removed, the cell pellet resuspended in Matrigel™ and seeded into pre-warmed cell culture plates. After ~ 20 min, the Matrigel™ was overlaid with the respective medium. The medium was changed twice per week, and the organoids were kept in a humidified incubator at 37°C and 5% CO_2.

Organoid stocks

Organoid stocks were prepared by releasing organoids from ~ 1-week-old fully formed organoid cultures, by dissolving them from Matrigel™ in cold ADF, pelleting by centrifugation, and resuspension in 500 μl of freezing medium CryoSFM. After transfer of the organoid suspension into cryotubes and a freezing container, stocks were kept for at least 24 h at −80°C before transfer into liquid nitrogen for long-term storage.

Production of Wnt3a- and RSPO1-conditioned medium

Two cell lines stably producing Wnt3a (L Wnt-3a cells) and R-Spondin 1 (293T HA Rspo1-Fc cells) were used for the production of conditional medium. The conditioned medium was produced based on a protocol modified from Willert *et al* (2003) and Farin *et al* (2012). In brief, cells were defrozen and seeded in DMEM with 10% FCS. The cells were passaged and selected with Zeocin (Invitrogen) at a final concentration of 125 μg/ml. After at least 5 days of selection, fresh DMEM with only 5% FCS was added. Upon incubation

for another 4–5 days, the supernatant was collected, centrifuged (1,200 × *g* for 10 min), filtered through a Steritop bottle (0.22 μm), aliquoted, and stored at −20°C. Conditioned medium from the parental L cell line was produced as a control in the same way, only without Zeocin selection. To determine the Wnt activity of the conditioned medium, the supernatants were added to a Wnt reporter cell line (293T WntR), which turns green, due to insertion of a plasmid carrying the GFP gene under control of a Wnt responsive element (7xTcf-eGFP; Addgene 24304; Fuerer *et al*, 2010). The quality of the conditioned medium was evaluated depending on the quantity and intensity of the GFP signal.

Cloning of shRNAs and virus production

To obtain stable knockdowns of PTEN and RB, shRNA sequences targeting specific regions within the respective mRNA (in-house-designed) were cloned into the lentiviral vector, pLVTHM, carrying mCherry, or GFP as mammalian selection marker (Appendix Table S5). Also, a shRNA against Luciferase cloned into pLVTHM-mCherry and-GFP was included as a control. The retroviral vector with the shRNA against p53 was provided by Alexander Loewer. Cloning and virus production involved the following steps:

1. The pLVTHM-GFP or pLVTHM-mCherry vectors were digested by *ClaI/MluI* (NEB) enzymatic restriction.
2. Sense and antisense oligos (target sequence with specific overhangs to generate hairpin structure; Appendix Table S4) were annealed using the following program in a thermocycler: (i) 94°C—4 min; (ii) 70°C—10 min; 70°C—1 s; (iii) 99 cycles of 69.9°C—1 s, 69.8°C—1 s, 69.7°C—1 s, 69.6°C—1 s; (iv) 20°C —99 s; (v) 10°C—60 s; and (vi) 4°C. Annealed oligos were diluted 1:200 in water.
3. Ligation of the linearized vector and annealed oligos was performed using the Quick ligation kit (NEB).
4. The ligation mix was transformed into chemically competent *E.coli Stbl3* by incubation for 20 min on ice, 2 min at 42°C, and 2 min on ice. After addition of 200 μl of LB medium, the bacteria were incubated for 1 h at 37°C on a shaker and the bacterial suspension was transferred to a LB agar plate supplemented with 100 mg/ml ampicillin and incubated ON at 37°C.
5. After successful transformation, bacterial clones were picked and grown in an ON culture. The next day, a plasmid prep (QIAGEN) and bacterial stocks were prepared.
6. To ensure that the oligos were inserted correctly into the plasmid, a control digestion with *KpnI/EcoRI* (NEB) enzymes was performed (30 min at 37°C).

Replication-deficient retroviral (RV) and lentiviral (LV) particles were produced by transient transfection of HEK 293T in 10-cm dishes:

1. Specific amounts of viral target plasmids (2.6 μg) as well as retro- and lentiviral packaging (1.95 μg) and envelope plasmids (0.65 μg) were mixed with Opti-MEM™ (Thermo Scientific) to achieve a final volume of 52 μl.
2. Next, a mixture of Opti-MEM™ and FuGENE® 6 (Promega) was added to the plasmids and incubated for 20–30 min at RT.
3. The formed liposomes were added dropwise to HEK 293T cells (~ 75% confluence) in 1×DMEM (supplemented with

2 mM L-glutamine, 1 mM Na-pyruvate, and 10% FCS).
4. The next day (~ 12 h), the transfection medium was aspirated and fresh medium added.
5. Around 36–48 h post-transfection, the viral supernatant was collected, filtered (0.45 μm), and concentrated with Lenti-X™ concentrator (Clontech).
6. The viral pellet was resuspended in ADF medium to achieve 10× concentrated virus. Aliquots were stored at −80°C.

Genetic manipulation of primary cells

1. Freshly isolated FTECs in 2D culture of an early passage (p0/p1) were transduced when reaching around 50–70% confluence with 1× concentrated retrovirus, carrying the p53 shRNA and puromycin selection marker, which was diluted in transduction medium (ADF + + supplemented with 5% FCS, 10 ng/ml hEGF, and 5 μg/μl polybrene (Sigma)).
2. The cells were incubated for 12–18 h with the virus. The next day, the supernatant was removed and fresh 2D medium was added to the cells.
3. When the cultures reached 80–90% confluence, they were split with TrypLE™ and seeded back into 2D at a ratio of 1:3.
4. In the next passage, the lentivirus carrying the PTEN shRNA and mCherry selection marker was added to the cells at 50–70% confluence in transduction medium. The cells were split again when reaching 90% confluence.
5. Cells were further sequentially transduced with the third viral vector carrying the shRNA against RB and the GFP selection marker. After culture reached 80–90% confluence in maximum passage 3, successfully transduced cells were selected.
6. To retrieve cells carrying a fluorescent selection marker, FACS was performed. For this purpose, the primary cells were detached using TrypLE™ (~ 10 min), pelleted by centrifugation (5 min, 300 × *g*), resuspended in FACS buffer (1×DPBS with 1% FCS, 1% HEPES, and 3% ROCK inhibitor), and passed through a 35-μm cell strainer into polystyrene tubes.
7. Propidium iodide (Sigma) was added shortly before FACS to exclude the dead cells. Sorting was performed by the Flow Cytometry Core Facility (DRFZ, Charitéplatz 1, 10117 Berlin) using the FACSAria II (BD). The GFP and mCherry single- or double-positive cells were collected in polystyrene tubes supplied with 2D medium (ADF with Glutamax, HEPES, 5% FCS, Pen/Strep, hEGF, and ROCK inhibitor).
8. Collected cells were centrifuged directly after FACS and seeded in 3D culture with around $1.5 × 10^5$ cells/50 μl Matrigel™. Cells transduced with the retroviral vector carrying the p53 shRNA were selected by adding 0.5 μg/ml puromycin (Gibco) for 10 days to the respective cell culture.

Single-cell preparation and flow cytometric analysis

1. To prepare single cells, organoids were released from Matrigel™ using cold PBS and pelleted by centrifugation (5 min, 300 × *g*).
2. The organoid pellet was resuspended in TrypLE™ and incubated for 15–20 min at 37°C.

3   After enzymatic treatment and vortexing (three times for 6 s), the organoid fragments were further mechanically disrupted by passing 3–4× through a needle (26G).

4   Next, the cells were taken up in ADF + + and passed through a 40-μm filter. The single-cell suspension was pelleted and washed by addition of 1% BSA/PBS.

5   The cells were stained in 2% BSA/PBS. Staining was performed for 10–30 min at 4°C in the dark. Finally, the cells were washed and resuspended in 1× PBS.

6   Flow cytometric analysis was performed using a FACSCanto™ II (BD) or LSRFortessa™ (BD) flow cytometer and the FlowJo vX.0.6 software.

Luminescent cell viability assay

To quantify the number of viable cells within one organoid well, the CellTiter-Glo® 3D Cell Viability Assay (Promega) was applied. According to the manufacturers' protocol, the organoids were lysed with the CellTiter-Glo® 3D reagent and the luminescence was measured within 30 min after the start of the reaction using black 96-well plates (Costar®, Corning) and a standard plate reader.

Immunohistochemistry of HGSOC tissue

Paraffin-embedded tumor samples in 5-μm sections were stained with antibodies against EpCam (Thermo Scientific), p16 (NeoMarkers), p53 (Dako), and Pax8 (Sigma) on the Ventana Benchmark XT Autostainer instrument. 3,3′-diaminobenzidine peroxide substrate (DAB$^+$) of the ultraView Universal DAB Detection Kit was used as a chromogen. The antibodies are well-established in the diagnostic routine laboratory, and signals were strong and clearly discernable.

Fixation, embedding, and immunofluorescence staining of organoids and tissue

For fixation, organoids were released from Matrigel™ and incubated in 3.7% PFA for ~ 1 h at RT, while tissue pieces were incubated in PFA for ~ 24 h at RT. Organoids and tissues were then dehydrated and paraffinized. For dehydration, organoids were passed manually through an alcohol dilution series: 60% EtOH (20 min, RT), 75% EtOH (20 min, RT), 90% EtOH (20 min, RT), abs. EtOH (20 min, RT), 100% isopropanol (20 min, RT), and 2 × 100% acetone (20 min, RT). Tissue pieces were transferred to the Shandon Citadell 1000 rondell for automatic dehydration. After dehydration, organoids and tissue pieces were embedded in paraffin, sectioned at 5 μm with a microtome (Microm), and collected onto microscope slides (Marienfeld).

Prior to staining, the formaldehyde-fixed paraffin-embedded (FFPE) organoids and tissues were deparaffinized by applying a series of decreasing alcohol concentrations: xylene (2 × 10 min), 100% ethanol (2 × 2 min), 90% ethanol (1 × 2 min), 70% ethanol (1 × 2 min), 50% ethanol (1 × 2 min), and H$_2$O (2 × 2 min). For antigen retrieval, the slides were incubated for 30 min at 98°C in 1× Target retrieval solution (Dako). Sections were stained by adding primary antibodies diluted in immunofluorescence buffer (IFB: 1% BSA, 2% FCS, and 0.1% Tween-20 in 1×PBS) and depending on the antibody incubated for 90 min at RT or overnight at 4°C in a humidified chamber. After washing 5 × 5 min with 1× PBS supplemented with 0.05% Tween-20, the respective secondary antibodies diluted in IFB together with the nucleic acid dye DRAQ5 or Hoechst were added to each section and incubated for 60 min at RT. Subsequently, the slides were washed and sections mounted with coverslips using Mowiol.

Hematoxylin and eosin staining

Before staining with hematoxylin and eosin (HE), organoid slices were deparaffinized as described above. After deparaffinization, the sections were covered completely with Mayer's haematoxylin solution (Roth) and incubated for 15 min at RT. The slides were rinsed with ddH$_2$O and tap water. Subsequently, the sections were covered with Eosin Y solution (1% aqueous, Roth) and incubated for 10 min at RT. Finally, slides were rinsed for 1 min with ddH2O and embedded using Roti®-Histokitt.

Quantitative reverse transcription–PCR (qRT–PCR)

The AB Power SYBR® Green RNA-to-CT™ 1-Step Kit (Thermo Fisher) was applied to perform reverse transcription and quantitative PCR in one step. RNA was added in a volume of 10 μl at a concentration between 2 and 10 ng/μl. qRT–PCR was performed using the StepOnePlus™ Real-Time PCR System (Applied Biosystems) with the following program: (i) 30 min, 48°C; (ii) 10 min, 95°C; (iii) 15 s, 95°C; and (iv) 1 min, 60°C. Steps 3 and 4 were repeated 40 times. For each primer pair and RNA-sample, the reaction was done in triplicate. The amplification plots obtained from the qRT–PCR were analyzed with the StepOne™ Software (version 2.3; Thermo Fisher). The expression levels were relatively quantified by calculating $\Delta\Delta C_t$, and the expression of the target genes was always normalized to the expression of the housekeeping gene glyceraldehyde-3-phosphate dehydrogenase (GAPDH).

Western blotting

For the purpose of sample collection, organoids were washed with DPBS, pelleted, and lysed by addition of 1× Laemmli buffer and heating for 10 min at 95°C. After the proteins were separated according to their molecular weight by performing SDS–PAGE, they were transferred from the gel to a PVDF membrane using a Mini Trans-Blot® Electrophoretic Transfer Cell (Bio-Rad) and applying 250 mA, 400 V, and 4°C under constant stirring for 2.5 h. After blocking in a 1:1 mixture of 5% milk and 5% BSA, the membrane was incubated at 4°C overnight with the primary antibody. The next day, the membrane was washed 3 × 10 min in TBS-0.1% Tween-20. Subsequently, the membrane was incubated for 1 h at RT with the respective conjugated secondary antibody. After washing, the membrane was covered with chemiluminescence reagents (Perkin Elmer). Using Hyperfilm (Amersham Biosciences) and a developer machine, the proteins were visualized. The housekeeping gene β-actin was used as the internal control for normalization of protein loading.

DNA and RNA isolation

DNA of tissue and organoids was isolated using the AllPrep DNA/RNA Mini Kit (QIAGEN) according to manufacturers' protocol. DNA purifications were quantified by measuring optical density at 260-nm wavelengths.

RNA from cells of 3D cultures was isolated using the RNeasy Mini Kit (QIAGEN) or the AllPrep DNA/RNA Mini Kit (QIAGEN). RNA from tissue samples was isolated using the AllPrep DNA/

RNA Mini Kit (QIAGEN). After pelleting the organoids, they were lysed in the respective sample buffer and RNA purification was performed according to the manufacturer's protocols. RNA concentration and purity were measured with a NanoDrop® ND-1000 Spectrophotometer.

For microarray analysis, total RNA was isolated with TRIzol (Life Technologies) according to the supplier's protocol using glycogen as carrier. Quality control and quantification of total RNA were carried out using the NanoDrop 1000 UV-Vis spectrophotometer (Kisker) as well as the Agilent 2100 Bioanalyzer with a RNA Nano 6000 microfluidics kit (Agilent Technologies).

Drug testing

To test the response of patient-derived HGSOC organoids to the chemotherapeutic drug carboplatin (Merck), organoids were dissociated into single cells by using enzymatic (TrypLE™, 15 min, 37°C) and mechanical (vortexing and passing through 26G needle) disruption. Subsequently, cells were counted and seeded at 15,000 cells/25 μl Matrigel™ into a 48-well plate. After maturation of organoids (~ 7–10 days in culture), treatment with carboplatin with a concentration range between 0 and 100 μg/ml was started. At 1 week post-treatment, cell viability was determined as described above.

Microarrays (dual-color and single-color)

Microarray experiments were performed as dual-color or single-color hybridizations on either Agilent Whole Human Genome 4 × 44K microarrays (Design ID 014850) or 8 × 60K human custom (Agilent-048908) microarrays comprising identical features for coding genes. Color-swap dye-reversal hybridizations were performed in order to compensate for dye-specific effects and to ensure statistically relevant data when using small sample sizes. RNA labeling was done either with a two-color Quick Amp Labeling Kit (4 × 44K arrays) or with a one-color Low Input Quick Amp Kit (8 × 60K arrays) according to the supplier's recommendations (Agilent Technologies).

In brief, mRNA was reverse transcribed and amplified using an oligo-dT-T7 promoter primer and the T7 RNA polymerase. The resulting cRNA was labeled with only Cyanine 3-CTP (single-color) or with Cyanine 3-CTP and Cyanine 5-CTP (dual-color). After precipitation, purification, and quantification, 1 μg (4 × 44K arrays) or 300 ng (8 × 60K arrays) of each labeled cRNA was fragmented and hybridized to whole-genome multipack microarrays according to the manufacturer's protocol (Agilent Technologies). Scanning of microarrays was performed with 5-μm resolution and XDR extended range (4 × 44K arrays) or 3-μm resolution (8 × 60K arrays) using a G2565CA high-resolution laser microarray scanner (Agilent Technologies). Microarray image data were analyzed and extracted with the Image Analysis/Feature Extraction software G2567AA v. A.11.5.1.1 (Agilent Technologies) using default settings and either the GE2_1100_Jul11 (dual-color) or the GE1_1105_Oct12 (single-color) extraction protocol.

For analysis of dual-color microarrays, the extracted MAGE-ML files were processed with the Rosetta Resolver, Build 7.2.2 SP1.31 (Rosetta Biosoftware). Ratio profiles comprising single hybridizations were combined in an error-weighted fashion to create ratio experiments. A 1.5-fold change expression cut-off for ratio experiments was applied together with anti-correlation of ratio profiles, rendering a highly significant, robust and reproducible microarray

analysis (*P*-value < 0.01). Additionally, raw data txt files were analyzed with R packages from the Bioconductor repository.

The extracted single-color raw data files were background corrected, quantile normalized, and further analyzed for differential gene expression using R 3.4 (Ritchie *et al*, 2015). Microarray gene expression comparisons between groups and the associated BioConductor package LIMMA were performed using unpaired tests for all human comparisons (R Core Team, 2013).

All microarray data have been deposited in the Gene Expression Omnibus (see Data availability section).

Capture of the targeted disease-related genome and next-generation sequencing

A SureSelectXT Automation Custom Capture Library (Agilent) target enrichment panel was designed. The enrichment panel comprised all coding exons of 121 genes associated with ovarian cancer (Table EV3). Capture was performed according to the manufacturer's instructions using an NGS Workstation Option B (Agilent) for automated library preparation starting with 3 μg DNA per sample. Sequencing was performed on an Illumina HiSeq 2500 system generating 2 × 100 bp paired-end reads with a target coverage of > 200-fold per sample. Sequence reads were mapped to the haploid human reference genome (hg19) using BWA. Single nucleotide variants (SNVs) and short insertions and deletions (indels) were called using FreeBayes v1.1. (preprint: Garrison & Marth, 2012). Sequencing data were deposited at the European Genome-phenome Archive (see Data availability section).

Variants called by FreeBayes were filtered for quality (QUAL > 10, coverage > 50) and annotated by SnpEff v4.3k (Cingolani *et al*, 2012) and Annovar (Wang *et al*, 2010). For each variant, the effect with the highest impact as defined by SnpEff was selected. Variants were flagged as rare if they showed < 1% population frequency in the 1,000 genome (Auton *et al*, 2015) and ESP6500 (Exome Variant Server, NHLBI GO Exome Sequencing Project (ESP), Seattle, URL: http://evs.gs.washington.edu/EVS/; accessed 2014-12) data sets. Predictions of amino acid exchange effects on protein function from MetaSVM, MetaLR, and M-CAP as provided by Annovar were used to assess loss of function.

Statistical analysis

Unless otherwise stated, two-sided Student's *t*-test was applied to determine statistical significance between two experimental groups and results are presented as the mean ± SEM (standard error of the mean) or mean ± SD (standard deviation). Analysis was performed with GraphPad Prism 7.03. A *P*-value ≤ 0.05 was considered statistically significant.

Data availability

All microarray data have been deposited in the Gene Expression Omnibus (GEO; www.ncbi.nlm.nih.gov/geo/) of the National Center for Biotechnology Information and can be accessed with the GEO accession numbers GSE125883 and GSE124766. Sequence data have been deposited at the European Genome-phenome Archive (EGA) under accession number EGAS00001003821 (https://www.ebi.ac.uk/ega/studies/EGAS00001003821). All code used for generating

analyses in this publication is available from https://github.com/ MPIIB-Department-TFMeyer/Hoffmann_et_al_Ovarian_Cancer_Orga noids.

Author contributions

MK and TFM conceived the project; MK and KH designed experiments, which were conducted by KH, MK, and ST; HK designed and planned targeted sequencing, which was performed by TZ; HB and TZ analyzed the targeted sequencing data. HB and H-JM analyzed microarray data. SD-E and ET performed pathology analysis of the tissue samples. MM selected patients and provided human FT samples. JS, EB and RC selected the patients, and provided material and clinical data of primary HGSOC patients. TFM supported the project financially; KH, MK, and TFM wrote the manuscript; MK and TFM supervised the project.

Conflict of interest

The authors declare that they have no conflict of interest.

References

Auton A, Brooks LD, Durbin RM, Garrison EP, Kang HM, Korbel JO, Marchini JL, McCarthy S, McVean GA, Abecasis GR (2015) A global reference for human genetic variation. *Nature* 526: 68–74

Bowtell DD, Bohm S, Ahmed AA, Aspuria PJ, Bast RC Jr, Beral V, Berek JS, Birrer MJ, Blagden S, Bookman MA *et al* (2015) Rethinking ovarian cancer II: reducing mortality from high-grade serous ovarian cancer. *Nat Rev Cancer* 15: 668–679

Brahmi M, Alberti L, Dufresne A, Ray-Coquard I, Cassier P, Meeus P, Decouvelaere AV, Ranchere-Vince D, Blay JY (2015) KIT exon 10 variant (c.1621 A>C) single nucleotide polymorphism as predictor of GIST patient outcome. *BMC Cancer* 15: 780

Brummelkamp TR, Bernards R, Agami R (2002) Stable suppression of tumorigenicity by virus-mediated RNA interference. *Cancer Cell* 2: 243–247

Callahan MJ, Crum CP, Medeiros F, Kindelberger DW, Elvin JA, Garber JE, Feltmate CM, Berkowitz RS, Muto MG (2007) Primary fallopian tube malignancies in BRCA-positive women undergoing surgery for ovarian cancer risk reduction. *J Clin Oncol* 25: 3985–3990

Cancer Genome Atlas Research Network (2011) Integrated genomic analyses of ovarian carcinoma. *Nature* 474: 609–615

Choi YJ, Ingram PN, Yang K, Coffman L, Iyengar M, Bai S, Thomas DG, Yoon E, Buckanovich RJ (2015) Identifying an ovarian cancer cell hierarchy regulated by bone morphogenetic protein 2. *Proc Natl Acad Sci USA* 112: E6882–E6888

Cingolani P, Platts A, le Wang L, Coon M, Nguyen T, Wang L, Land SJ, Lu X, Ruden DM (2012) A program for annotating and predicting the effects of single nucleotide polymorphisms, SnpEff: SNPs in the genome of *Drosophila melanogaster* strain w1118; iso-2; iso-3. *Fly (Austin)* 6: 80–92

Ducie J, Dao F, Considine M, Olvera N, Shaw PA, Kurman RJ, Shih IM, Soslow RA, Cope L, Levine DA (2017) Molecular analysis of high-grade serous ovarian carcinoma with and without associated serous tubal intra-epithelial carcinoma. *Nat Commun* 8: 990

Farin HF, Van Es JH, Clevers H (2012) Redundant sources of wnt regulate intestinal stem cells and promote formation of paneth cells. *Gastroenterology* 143: 1518–1529.e7

Fuerer C, Nusse R (2010) Lentiviral vectors to probe and manipulate the Wnt signaling pathway. *PLoS One* 5: e9370

Fujii M, Shimokawa M, Date S, Takano A, Matano M, Nanki K, Ohta Y, Toshimitsu K, Nakazato Y, Kawasaki K *et al* (2016) A colorectal tumor organoid library demonstrates progressive loss of niche factor requirements during tumorigenesis. *Cell Stem Cell* 18: 827–838

Gao MQ, Choi YP, Kang S, Youn JH, Cho NH (2010) CD24(+) cells from hierarchically organized ovarian cancer are enriched in cancer stem cells. *Oncogene* 29: 2672–2680

Garrison E, Marth G (2012) Haplotype-based variant detection from short-read sequencing. *arXiv* 1207.3907 [q-bio.GN] [PREPRINT]

Ghosh A, Syed SM, Tanwar PS (2017) *In vivo* genetic cell lineage tracing reveals that oviductal secretory cells self-renew and give rise to ciliated cells. *Development* 144: 3031–3041

Hill SJ, Decker B, Roberts EA, Horowitz NS, Muto MG, Worley MJ Jr, Feltmate CM, Nucci MR, Swisher EM, Nguyen H *et al* (2018) Prediction of DNA repair inhibitor response in short-term patient-derived ovarian cancer organoids. *Cancer Discov* 8: 1404–1421

Huber MA, Kraut N, Beug H (2005) Molecular requirements for epithelial-mesenchymal transition during tumor progression. *Curr Opin Cell Biol* 17: 548–558

Jazaeri AA, Bryant JL, Park H, Li H, Dahiya N, Stoler MH, Ferriss JS, Dutta A (2011) Molecular requirements for transformation of fallopian tube epithelial cells into serous carcinoma. *Neoplasia* 13: 899–911

Kalender ME, Demiryurek S, Oztuzcu S, Kizilyer A, Demiryurek AT, Sevinc A, Dikilitas M, Yildiz R, Camci C (2010) Association between the Thr431Asn polymorphism of the ROCK2 gene and risk of developing metastases of breast cancer. *Oncol Res* 18: 583–591

Karst AM, Levanon K, Drapkin R (2011) Modeling high-grade serous ovarian carcinogenesis from the fallopian tube. *Proc Natl Acad Sci USA* 108: 7547–7552

Kessler M, Hoffmann K, Brinkmann V, Thieck O, Jackisch S, Toelle B, Berger H, Mollenkopf HJ, Mangler M, Sehouli J *et al* (2015) The Notch and Wnt pathways regulate stemness and differentiation in human fallopian tube organoids. *Nat Commun* 6: 8989

Kopper O, de Witte CJ, Lohmussaar K, Valle-Inclan JE, Hami N, Kester L, Balgobind AV, Korving J, Proost N, Begthel H *et al* (2019) An organoid platform for ovarian cancer captures intra- and interpatient heterogeneity. *Nat Med* 25: 838–849

Kryczek I, Liu S, Roh M, Vatan L, Szeliga W, Wei S, Banerjee M, Mao Y, Kotarski J, Wicha MS *et al* (2012) Expression of aldehyde dehydrogenase and CD133 defines ovarian cancer stem cells. *Int J Cancer* 130: 29–39

Kuchenbaecker KB, Ramus SJ, Tyrer J, Lee A, Shen HC, Beesley J, Lawrenson K, McGuffog L, Healey S, Lee JM *et al* (2015) Identification of six new susceptibility loci for invasive epithelial ovarian cancer. *Nat Genet* 47: 164–171

Kuhn E, Kurman RJ, Vang R, Sehdev AS, Han G, Soslow R, Wang TL, Shih Ie M (2012) TP53 mutations in serous tubal intraepithelial carcinoma and concurrent pelvic high-grade serous carcinoma—evidence supporting the clonal relationship of the two lesions. *J Pathol* 226: 421–426

Lee Y, Miron A, Drapkin R, Nucci MR, Medeiros F, Saleemuddin A, Garber J, Birch C, Mou H, Gordon RW *et al* (2007) A candidate precursor to serous carcinoma that originates in the distal fallopian tube. *J Pathol* 211: 26–35

Leeper K, Garcia R, Swisher E, Goff B, Greer B, Paley P (2002) Pathologic findings in prophylactic oophorectomy specimens in high-risk women. *Gynecol Oncol* 87: 52–56

Lupia M, Cavallaro U (2017) Ovarian cancer stem cells: still an elusive entity? *Mol Cancer* 16: 64

Mao BY, Wu W, Davidson G, Marhold J, Li MF, Mechler BM, Delius H, Hoppe D, Stannek P, Walter C *et al* (2002) Kremen proteins are Dickkopf receptors that regulate Wnt/beta-catenin signalling. *Nature* 417: 664–667

Maru Y, Tanaka N, Itami M, Hippo Y (2019) Efficient use of patient-derived organoids as a preclinical model for gynecologic tumors. *Gynecol Oncol* 154: 189–198

McLean K, Gong Y, Choi Y, Deng N, Yang K, Bai S, Cabrera L, Keller E, McCauley L, Cho KR *et al* (2011) Human ovarian carcinoma-associated mesenchymal stem cells regulate cancer stem cells and tumorigenesis via altered BMP production. *J Clin Invest* 121: 3206–3219

Nakamura K, Banno K, Yanokura M, Iida M, Adachi M, Masuda K, Ueki A, Kobayashi Y, Nomura H, Hirasawa A *et al* (2014) Features of ovarian cancer in Lynch syndrome (Review). *Mol Clin Oncol* 2: 909–916

Nakamura K, Nakayama K, Ishikawa N, Ishikawa M, Sultana R, Kiyono T, Kyo S (2018) Reconstitution of high-grade serous ovarian carcinoma from primary fallopian tube secretory epithelial cells. *Oncotarget* 9: 12609–12619

Neal JT, Li X, Zhu J, Giangarra V, Grzeskowiak CL, Ju J, Liu IH, Chiou SH, Salahudeen AA, Smith AR *et al* (2018) Organoid modeling of the tumor immune microenvironment. *Cell* 175: 1972–1988.e16

Norquist BM, Brady MF, Harrell MI, Walsh T, Lee MK, Gulsuner S, Bernards SS, Casadei S, Burger RA, Tewari KS *et al* (2018) Mutations in homologous recombination genes and outcomes in ovarian carcinoma patients in GOG 218: an NRG Oncology/Gynecologic Oncology Group Study. *Clin Cancer Res* 24: 777–783

Ozdamar B, Bose R, Barrios-Rodiles M, Wang HR, Zhang Y, Wrana JL (2005) Regulation of the polarity protein Par6 by TGFbeta receptors controls epithelial cell plasticity. *Science* 307: 1603–1609

Phan N, Hong JJ, Tofig B, Mapua M, Elashoff D, Moatamed NA, Huang J, Memarzadeh S, Damoiseaux R, Soragni A (2019) A simple high-throughput approach identifies actionable drug sensitivities in patient-derived tumor organoids. *Commun Biol* 2: 78

R Core Team (2013) *R: a language and environment for statistical computing*. Vienna, Austria: R Foundation for Statistical Computing. https://wwwR-project.org/

Reid BM, Permuth JB, Sellers TA (2017) Epidemiology of ovarian cancer: a review. *Cancer Biol Med* 14: 9–32

Ritchie ME, Phipson B, Wu D, Hu Y, Law CW, Shi W, Smyth GK (2015) limma powers differential expression analyses for RNA-sequencing and microarray studies. *Nucleic Acids Res* 43: e47

Seino T, Kawasaki S, Shimokawa M, Tamagawa H, Toshimitsu K, Fujii M, Ohta Y, Matano M, Nanki K, Kawasaki K *et al* (2018) Human pancreatic tumor organoids reveal loss of stem cell niche factor dependence during disease progression. *Cell Stem Cell* 22: 454–467.e6

Vaughan S, Coward JI, Bast RC Jr, Berchuck A, Berek JS, Brenton JD, Coukos G, Crum CC, Drapkin R, Etemadmoghadam D *et al* (2011) Rethinking ovarian cancer: recommendations for improving outcomes. *Nat Rev Cancer* 11: 719–725

Wang K, Li M, Hakonarson H (2010) ANNOVAR: functional annotation of genetic variants from high-throughput sequencing data. *Nucleic Acids Res* 38: e164

Willert K, Brown JD, Danenberg E, Duncan AW, Weissman IL, Reya T, Yates JR, Nusse R (2003) Wnt proteins are lipid-modified and can act as stem cell growth factors. *Nature* 423: 448–452

Yang BK, Yan XB, Liu LG, Jiang CY, Hou SP (2017a) Overexpression of the cancer stem cell marker CD117 predicts poor prognosis in epithelial ovarian cancer patients: evidence from meta-analysis. *Oncotargets Ther* 10: 2951–2961

Yang XH, Tang F, Shin J, Cunningham JM (2017b) A c-Myc-regulated stem cell-like signature in high-risk neuroblastoma: a systematic discovery (Target neuroblastoma ESC-like signature). *Sci Rep* 7: 41

Yue W, Sun Q, Dacic S, Landreneau RJ, Siegfried JM, Yu J, Zhang L (2008) Downregulation of Dkk3 activates beta-catenin/TCF-4 signaling in lung cancer. *Carcinogenesis* 29: 84–92

Zhang Y, Cao L, Nguyen D, Lu H (2016) TP53 mutations in epithelial ovarian cancer. *Transl Cancer Res* 5: 650–663